Geochimica et Cosmochimica Acta 400 (2025) 172–189

Contents lists available at ScienceDirect

Geochimica et Cosmochimica Acta

journal homepage: www.elsevier.com/locate/gca

Combined Ca, Sr isotope and trace element analyses of Late Cretaceous dinosaur teeth: assessing diet *versus* diagenesis

Mateusz M. Michailow [a], Federico Lugli [a,b,c,*], Anna Cipriani [a,d], Francesco Della Giustina [e], Annalisa Ferretti [a,**], Daniele Malferrari [a], Denver Fowler [f], Elizabeth Freedman Fowler [f,g], Michael Weber [h], Thomas Tütken [h]

[a] *Department of Chemical and Geological Sciences, University of Modena and Reggio Emilia, Via Campi 103, 41125 Modena, Italy*
[b] *Institute of Geosciences, Goethe University Frankfurt, Altenhöferallee 1, 60438 Frankfurt, Germany*
[c] *Department of Cultural Heritage, University of Bologna, Via degli Ariani 1, 48121 Ravenna, Italy*
[d] *Lamont-Doherty Earth Observatory of Columbia University, 61 Route 9W, 10964 Palisades, NY, USA*
[e] *Evolution and Diversity Dynamics Lab, Université de Liège, 14 Allée du 6 Août, 4000 Liège, Belgium*
[f] *Badlands Dinosaur Museum, Dickinson Museum Center, 188 Museum Dr. E., Dickinson, ND 58601, USA*
[g] *School of Applied Sciences, Dickinson State University, Dickinson, ND 58601, USA*
[h] *Institute of Geosciences, Johannes Gutenberg University, 55128 Mainz, Germany*

ARTICLE INFO

Associate editor: Elizabeth Morris Griffith

Keywords:
Non-traditional stable isotopes
Rare earth elements
Enamel
Trophic ecology
Dinosaurs

ABSTRACT

The Sr and Ca isotope composition, along with trace element content in fossil teeth, provides valuable insights into biogenic and diagenetic processes. Identifying pristine biological signals is crucial for reconstructing the diet and trophic levels of extinct taxa. We present novel geochemical data from Tyrannosauridae and Ceratopsidae teeth of the Late Cretaceous, using radiogenic Sr ($^{87}Sr/^{86}Sr$), stable Sr ($\delta^{88/86}Sr$), and Ca ($\delta^{44/42}Ca$) isotopes, along with trace elements abundances to differentiate biogenic signals from diagenetic alteration.

Our results reveal potential taxon-specific diagenetic effects, likely influenced by enamel microstructure. Tyrannosaurid enamel contains lower concentrations of rare earth elements (REE) and uranium (U) than dentine, whereas ceratopsid teeth typically exhibit higher REE and U compared to both the enamel and dentine of tyrannosaurids. Enamel $\delta^{44/42}Ca$ values differ significantly between herbivorous ceratopsids and carnivorous tyrannosaurids, reflecting trophic level effects seen in modern mammals and reptiles. A positive correlation between $\delta^{44/42}Ca$ and $\delta^{88/86}Sr$ suggests partial preservation of biological fractionation along the trophic chain. Yet, the lack of negative $\delta^{88/86}Sr$ values in our dataset – typically expected in biologic tissues – suggests alteration by diagenetic processes of both stable and radiogenic Sr. While $\delta^{44/42}Ca$ in enamel likely remains a reliable dietary proxy, Sr isotope composition of our samples appears then to be significantly altered. The presence of high $\delta^{88/86}Sr$ in terrestrial fossil teeth could serve as a novel diagenetic proxy to assess habitat related $^{87}Sr/^{86}Sr$ values, aiding provenance and mobility studies in fossil ecosystems.

1. Introduction

Fossil biological hard tissues of vertebrates serve as exceptional archives of extinct organisms and past ecosystems (e.g., Gannes et al., 1998; Newsome et al., 2010; Clementz, 2012). Dinosaur teeth, in particular, are remarkable for deciphering feeding habits and ethology of these animals, providing dietary insights beyond what morphology alone can reveal. While tooth shape, microwear, and enamel-dentine microstructures provide clues to taxonomic and dietary identification (Currie et al., 1990; Erickson et al., 2012; Fiorillo and Currie, 1994; Hwang, 2010, 2011; Mallon and Anderson, 2014; LeBlanc et al., 2020; Ballell et al., 2022), teeth bioapatite preserves trace elements and isotope compositions linked to mobility, diet, trophic level, and feeding habits in both extant and extinct vertebrate taxa (see, among others, Skulan and DePaolo, 1999; Kohn and Cerling, 2002; Hedges et al., 2006; Koch, 2007; Reynard et al., 2010, 2011; Heuser et al., 2011; Tacail et al., 2014, 2020; Martin et al., 2015, 2017, 2018, 2022; Jaouen and Pons, 2017; Hassler et al., 2018; Balter et al., 2019). However, extensive

---

* Corresponding author at: Department of Chemical and Geological Sciences, University of Modena and Reggio Emilia, Via Campi 103, 41125 Modena, Italy.
** Corresponding author.
E-mail addresses: federico.lugli@unimore.it (F. Lugli), annalisa.ferretti@unimore.it (A. Ferretti).

https://doi.org/10.1016/j.gca.2025.05.006
Received 12 July 2024; Accepted 5 May 2025

characterization is needed to distinguish geochemical biogenic signals from post-depositional alteration. This is because shortly after burial, vertebrate skeletal remains undergo taphonomic processes that alter their chemical composition, affecting the original elemental and isotopic signature. These changes occur as elements and isotopes of the *in-vivo* signal interact with pore fluids at different temperatures and chemical conditions (e.g., Kohn et al., 1999; Trueman and Tuross, 2002; Weber et al., 2021; Kral et al., 2022).

The mineral phase of teeth consists of small, non-stoichiometric carbonate-hydroxylapatite crystallites (Weiner and Price, 1986; Kohn et al., 1999; Trueman and Tuross, 2002; Trueman et al., 2003, 2008; Pasteris et al., 2008; Tütken and Vennemann, 2011). After death, the organic matrix is lost, and bioapatite recrystallizes from metastable nm-sized biogenic crystals into larger thermodynamically more stable inorganic apatite minerals such as carbonate-fluorapatite, incorporating trace elements from the environment (Hubert et al., 1996; Kolodny et al., 1996; Trueman and Tuross, 2002; Trueman et al., 2003, 2008; Pfretzschner, 2004; Tütken and Vennemann, 2011; Kral et al., 2022, 2024). This process reduces porosity but does not eliminate all empty spaces (Trueman and Tuross, 2002; Gueriau et al., 2014). The high porosity and small apatite crystals of dentine tissue render it particularly susceptible to diagenetic alteration, whereas the low organic content and tightly packed larger crystals of enamel provide enhanced resistance (Thorp and Vandermerwe, 1987; Wang and Cerling, 1994; Kohn et al., 1999; Sharp et al., 2000; Kohn and Cerling, 2002; Fricke et al., 2008; Heuser et al., 2011; Tütken and Vennemann, 2011; Montanari et al., 2013). For paleoecological interpretations it is therefore crucial to obtain a robust set of complementary geochemical proxies to assess diagenetic alteration and ensure data reliability. High field strength element (HFSE) abundances in bioapatite have long been used to reconstruct paleoenvironmental and taphonomic conditions with high concentrations generally reflecting *post mortem* alteration and chemical exchange with pore fluids in sediments (Trueman et al., 2006; Herwartz et al., 2011; Kowal-Linka et al., 2014; Kocsis et al., 2016). Dietary habits of fossil species instead are derived from Sr/Ca ratios (Elias et al., 1982; Burton et al., 1999; Balter, 2004), and isotope ratios of elements that are systematically fractionated along the food chain, such as C and N (Minagawa and Wada, 1984; Leichliter et al., 2021, 2023), or other, non-traditional isotopes such as those of Sr, Zn and Ca (for comprehensive reviews see Gannes et al., 1998; Lee-Thorp and Sponheimer, 2006; Koch, 2007; Newsome et al., 2010; Clementz, 2012; Jaouen and Pons, 2017; Martin et al., 2017; Tacail et al., 2020).

Several studies of living and fossil organisms suggest that Ca isotopes are a good indicator of diet and trophic level (Skulan et al., 1997; Skulan and DePaolo, 1999; Reynard et al., 2010, 2011; Tacail et al., 2014, 2020; Martin et al., 2015, 2017, 2018, 2022; Jaouen and Pons, 2017; Hassler et al., 2018; Balter et al., 2019; Cullen et al., 2022). Calcium plays a crucial role in the physiology of both vertebrates and invertebrates as it is a vital nutrient and the major element in their hard tissues. Ca phosphate, or bioapatite, is the major mineral phase present in bone, tooth enamel and dentine, with Ca concentrations up to 40 % wt (Heuser et al., 2011; Martin et al., 2017; Hassler et al., 2018). This makes Ca isotope composition relatively insensitive to diagenetic changes, allowing the reconstruction of diet-related Ca isotope compositions from bioapatite of million-year-old vertebrate fossils (Heuser et al., 2011; Dodat et al., 2023).

Metabolic and physiological processes regulate Ca distribution in living organisms, causing systematic isotope fractionation (i.e., decrease of $\delta^{44/42}$Ca values with each trophic level) between different tissues and taxa during trophic interaction, the so-called trophic level effect (Skulan et al., 1997; Skulan and DePaolo, 1999; Clementz et al., 2003; Martin et al., 2018). Teeth display systematically lower $\delta^{44/42}$Ca values than ingested dietary Ca because of considerable isotope fractionation during physiological processes such as renal function and biomineralization processes (Tacail et al., 2020). Herbivores display higher $\delta^{44/42}$Ca values than carnivores due to the nature of their diet. Notably, even a small intake (about 1–2 %) of mineralized tissue (i.e., bone rich in Ca depleted in ^{44}Ca) from a prey produces an even lower Ca isotope composition in the predator (Heuser et al., 2011). Therefore, through the food chain the $\delta^{44/42}$Ca values become systematically more negative at each consumer level (from plants to herbivores, to carnivores). Several studies on dinosaur teeth have shown that $\delta^{44/42}$Ca differs between dinosaur taxonomic groups (Martin et al., 2017, 2022; Hassler et al., 2018) with clear evidence of niche partitioning of apex predators at the top of the food chain.

Among herbivores, animals with a plant-based diet can be grouped into browsers and grazers. Browsers feed on high-growing plants and leaves, while grazers prefer grass and herbaceous low-growing vegetation. This distinction is reflected in their Ca isotope signatures due to complex fractionation processes in plants. In plant roots, cation-exchange processes favor lighter Ca isotopes, causing isotopic fractionation that results in leaves and stems being enriched in the heavier ^{44}Ca isotope relative to the roots (Cobert et al., 2011; Schmitt et al., 2012; Moynier and Fujii, 2017; Martin et al., 2018). Consequently, high growing plants (eaten by browsers) have higher $\delta^{44/42}$Ca values compared to low growing plants (eaten by grazers). This isotopic pattern is observable up the food chain. For example, Martin et al. (2022) found that hadrosaurids from Alberta, which likely foraged on tall plants, had enamel enriched in ^{44}Ca, whereas ceratopsids likely preferred low-growing plants.

Tyrannosaurids, renowned for their flesh-eating and bone-crushing behaviour, also consumed substantial amounts of hard tissues (Chin et al., 1998; Erickson et al., 1996; Gignac and Erickson, 2017). This is supported by studies of bone-bearing coprolites from Late Cretaceous North American tyrannosaurids (Chin et al., 1998, 2003). These coprolites contain a high percentage (30–50 %) of bone fragments (Chin et al., 1998) and other secondarily mineralized tissues. The latter represent initially non-mineralized soft tissues, such as muscle cells and connective tissue, that are phosphatized during diagenesis (Chin et al., 2003). The intake of significant amounts of hard tissues could drive Ca isotope signatures of tyrannosaurids to even lower values.

Strontium, although a non-essential trace element, follows biological pathways similar to Ca due to their comparable chemical properties. Along the food chain, the biopurification of Sr results in decreasing Sr/Ca ratios at higher trophic levels (Elias et al., 1982; Burton et al., 1999; Balter, 2004). Initially released from rocks and soils by erosion and weathering, Sr is absorbed by plants and subsequently incorporated into consumers, where it substitutes Ca during the formation of bioapatite (Bentley, 2006; Martin et al., 2017). Radiogenic Sr isotopes (^{87}Sr/^{86}Sr) thus serve as geochemical provenance tracers linking organism to the geological characteristics of the environment and enabling mobility assessment over an individual lifetime (e.g., Hoppe et al., 1999; Bentley, 2006; Knudson et al., 2010; Martin et al., 2017; Lugli et al., 2018, 2019; Wooller et al., 2021; Rowe et al., 2024). By comparing ^{87}Sr/^{86}Sr ratios in tooth enamel, which commonly mineralizes during early life (e.g. in mammals), with those in mature skeletal tissues, it is possible to trace migration across isotopically distinct geological substrates (Ericson, 1985; Bentley, 2006; Kocsis et al., 2009; Fischer et al., 2012; Martin et al., 2016; Terrill et al., 2020; Cullen et al., 2022).

Stable Sr isotopes (^{88}Sr/^{86}Sr), similarly to Ca isotopes, are increasingly used in paleodietary studies as trophic level proxies due to their mass-dependent fractionation along the food chain (Knudson et al., 2010; Tütken et al., 2015). Carnivores exhibit lower $\delta^{88/86}$Sr values than herbivores due to the preferential assimilation of ^{86}Sr in biological systems. Bedrock and soil samples generally display higher $\delta^{88/86}$Sr values than the dietary $\delta^{88/86}$Sr values, which may be altered through weathering (e.g., De Souza et al., 2010; Chao et al., 2015). These geogenic values decrease progressively as Sr moves from soils to plants (De Souza et al., 2010), and through the food chain reaching their lowest values in carnivores (Tütken et al., 2015).

In this study, we apply a multi-proxy geochemical approach, combining $\delta^{44/42}$Ca, ^{87}Sr/^{86}Sr, $\delta^{88/86}$Sr and trace element analysis, to teeth from two distinct dinosaur clades: herbivorous Ceratopsidae and carnivorous Tyrannosauridae. Our goal is to assess whether dietary Ca and Sr isotope signatures are preserved or have been diagenetically modified, allowing us to disentangle dietary from *post mortem* geochemical signals. By analyzing samples from nearby microsites within the same stratigraphic levels of the Judith River Formation (Montana, USA), we minimize geological, stratigraphic and taphonomic differences.

2. Geological setting

This study focuses on a collection of tooth fragments collected from multiple sites of the Judith River Formation, which is part of the Judith River-Belly River clastic wedge complex (Rogers et al., 2023; Eberth, 2024). This wedge consists of eastward thinning non-marine, paralic and marine facies, recording the cycling regression and transgression of the western shoreline of the Western Interior Seaway, an inland sea spanning from the modern Arctic to the proto-Gulf of Mexico, during the Late Cretaceous (Campanian) (Kauffman, 1984; Rogers et al., 2016, 2023; Eberth, 2024). The wedge complex (Fig. 1) extends from southern Alberta to eastern Saskatchewan in Canada (Belly River Group) and through northcentral Montana in the United States (Judith River Formation and Two Medicine Formation). It is constrained above and below by marine shales of the Bearpaw and Claggett formations, respectively (Rogers, 1998; Rogers et al., 2016, 2023).

The Judith River Formation is a vast sedimentary and fossiliferous Upper Cretaceous unit bounded at the base by shallow-marine facies (Parkman Sandstone Member), overlain by terrestrial deposits (McClelland Ferry Member) (Fowler, 2017). In western Montana, the Judith River Formation and the Two Medicine Formation are broadly coeval, with the latter spanning a longer time period. The Two Medicine Formation represents the landward portion of the depositional wedge, while the Judith River corresponds to the seaward, more marine influenced sector (Rogers et al., 2016).

The Judith River Formation is a widely distributed yet stratigraphically complex unit due to geographic variability, patchy outcrops, and tectonic disruption. It is correlated with the Belly River Group in Canada and subdivided into the Foremost, Oldman and Dinosaur Park Formations (Eberth and Hamblin, 1993; Jerzykiewicz and Norris, 1994; Hamblin and Abrahamson, 1996; Eberth, 2005, 2024; Rogers et al., 2016, 2023). The Foremost Formation is the oldest unit and includes paralic to non-marine facies with upward coarsening parasequences characteristic of a regression phase (Eberth, 2005). The overlying Oldman Formation records the Campanian maximum regression of the Western Interior Seaway, with alluvial and fluvial deposits (Eberth, 2005) under a warm, seasonally dry climate with high-energy rivers and low accumulation rates hindering fossil preservation (Rogers et al., 2016). Its upper contact, the Judith River-Belly River discontinuity, marks a rapid transgression (Eberth, 2005, 2024). The Dinosaur Park Formation, which overlies this discontinuity, records the last major transgression (Eberth, 2005) with estuarine and coastal deposits indicative of a warm, waterlogged environment, that enhanced high burial rates and increased fossil preservation (Rogers et al., 2016). Different vertebrate fossils have been reported from the Judith River Formation, including fishes, amphibians, turtles, crocodilians, birds, mammals, and dinosaurs. Among others, this formation has yielded theropods, ankylosaurs, ornithopods, pachycephalosaurs and ceratopsids (Sahni, 1972).

3. Materials

This study focuses on a collection of tooth fragments from Ceratopsidae and Tyrannosauridae from multiple sites of the Judith River Formation (Fig. 1). Tyrannosaurids, meat-eating theropod dinosaurs, were at the top of the food chain in North American and Asian ecosystems during the Late Cretaceous. This apex predator was characterized by a large robust skull, and extremely large and powerful neck muscles,

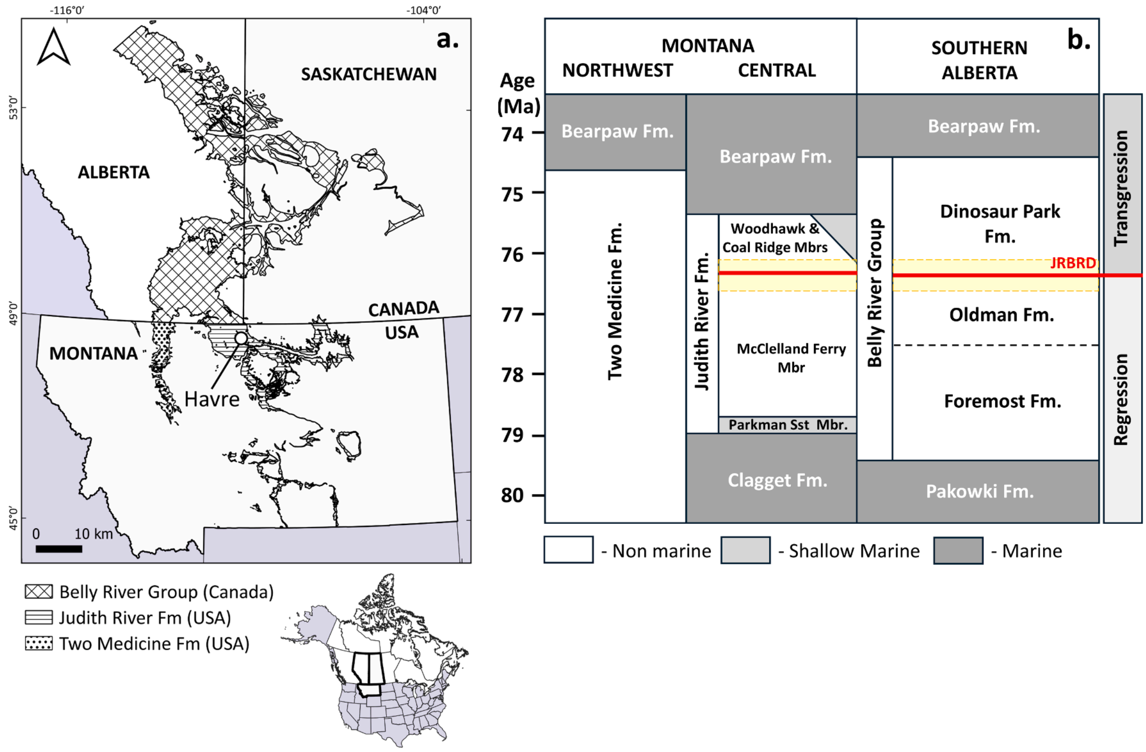

Fig. 1. (a) Geographic extension of the Judith River Formation (parallel lines pattern) and the Two Medicine Formation (dotted pattern) in Montana (USA), and the stratigraphically equivalent Belly River Group (cross line pattern), in Alberta and Saskatchewan (Canada). Samples' microsites are located near Havre (decimal degrees: lat. 48.69, long. −110.01). (b) Stratigraphic model of the Judith River Fm. and Belly River Group; yellow area represents the time-interval of the studied dinosaur teeth; red line is the Judit River-Belly River discontinuity (modified after Ramezani et al., 2022; Rogers et al., 2023; Eberth, 2024).

which together with the morphology of their serrated teeth, indicate that their hunting method was nearly completely based on the strength of their bite (Gignac and Erickson, 2017). As suggested by the presence of bite marks (Erickson et al., 1996; Jacobsen, 1998; Hone et al., 2018; Martin et al., 2022), and by ornithischian bone fragments in well-preserved coprolites (Chin et al., 1998), these theropods used to prey, among others, on medium-sized ornithischian herbivorous dinosaurs such as hadrosaurids and ceratopsids. This is also supported by spatial niche partitioning analysis of North American dinosaur fossil assemblages from the latest Cretaceous (Maastrichtian, Lyson and Longrich, 2011), that supports the co-occurrence of tyrannosaurids and both hadrosaurids and ceratopsids in the same habitats. The presence of bite marks on a small percentage of tyrannosaurid and other theropod bones might even indicate some cannibalistic behaviors (i.e., consumption of conspecifics) or occasional theropod feeding (Jacobsen, 1998; Martin et al., 2022).

Ceratopsids were medium-sized quadrupedal, horned plant-eating ornithischian dinosaurs, that thrived alongside tyrannosaurids in

Table 1
List of samples and Ca isotope composition of tyrannosaurid and ceratopsid teeth analyzed in this study. Teeth are grouped by sampling site and arranged by stratigraphic position (UMO: Uppermost Oldman; UO: Upper Oldman; LDP: Lower Dinosaur Park; ODPB: Oldman/Dinosaur Park boundary). The calcium isotope values are relative to NIST 915a. When n = 1, σ is the in-run error calculated as standard deviation; when n > 1, σ is the propagated uncertainty of the replicas' standard deviation and the average in-run error.

Stratigraphic Position	Site	Taxon	Tissue	Sample	$\delta^{44/42}$Ca (‰)	$\delta^{44/42}$Ca σ (‰)	$\delta^{43/42}$Ca (‰)	$\delta^{43/42}$Ca σ (‰)	n
LDP	Bullet micro	Ceratopsidae	enamel	1_2	−0.09	0.05	−0.10	0.07	1
LDP	Bullet micro	Ceratopsidae	enamel	1_3	−0.19	0.04	−0.07	0.09	1
LDP	Bullet micro	Tyrannosauridae	enamel	1_1	−0.32	0.05	−0.22	0.08	1
LDP	Bullet micro	Tyrannosauridae	enamel	1_4	−0.47	0.03	−0.24	0.08	1
LDP	Bullet micro	Tyrannosauridae	enamel	1_5	−0.38	0.05	−0.15	0.10	1
LDP	Denver side micro	Ceratopsidae	enamel	2_3	−0.63	0.05	−0.38	0.12	1
LDP	Denver side micro	Ceratopsidae	enamel	2_4	−0.02	0.07	−0.01	0.16	2
LDP	Denver side micro	Tyrannosauridae	enamel	2_1	−0.60	0.03	−0.29	0.09	1
LDP	Denver side micro	Tyrannosauridae	enamel	2_2	−0.40	0.03	−0.22	0.07	1
LDP	Jack's bonebed	Ceratopsidae	enamel	13_2	−0.35	0.05	−0.14	0.09	1
LDP	Jack's bonebed	Tyrannosauridae	enamel	13_1	−0.35	0.06	−0.07	0.08	1
LDP	Jack's bonebed	Tyrannosauridae	dentine	13_1	−0.10	0.05	−0.01	0.14	2
LDP	Jack's bonebed	Tyrannosauridae	enamel	13_3	−0.68	0.14	−0.34	0.10	3
LDP	Jack's side micro	Ceratopsidae	enamel	4_1	−0.36	0.13	−0.17	0.09	2
LDP	Jack's side micro	Ceratopsidae	enamel	4_2	−0.33	0.05	−0.20	0.12	2
LDP	Jack's side micro	Ceratopsidae	enamel	4_3	−0.17	0.14	−0.11	0.14	2
LDP	Jack's side micro	Ceratopsidae	dentine	4_3	−0.07	0.06	−0.06	0.10	2
LDP	Last side micro	Ceratopsidae	enamel	8_1	−0.51	0.22	−0.30	0.15	3
LDP	Last side micro	Tyrannosauridae	enamel	8_2	−0.59	0.04	−0.29	0.10	1
LDP	Nanoraptor micro	Ceratopsidae	enamel	5_1	0.25	0.11	0.13	0.23	2
LDP	Nanoraptor micro	Ceratopsidae	enamel	5_2	−0.56	0.05	−0.48	0.08	1
LDP	Nanoraptor micro	Ceratopsidae	dentine	5_2	−0.15	0.07	−0.05	0.13	2
LDP	Nanoraptor micro	Ceratopsidae	enamel	5_3	−0.55	0.17	−0.28	0.14	3
ODPB	All crew micro	Ceratopsidae	enamel	14_1	−0.22	0.10	−0.13	0.13	2
ODPB	All crew micro	Tyrannosauridae	enamel	14_3	−0.26	0.05	−0.15	0.08	1
ODPB	All crew micro	Tyrannosauridae	dentine	14_3	−0.12	0.08	−0.06	0.11	2
ODPB	High side micro	Ceratopsidae	enamel	12_1	−0.15	0.06	−0.11	0.13	1
ODPB	High side micro	Ceratopsidae	enamel	12_4	−0.13	0.06	0.00	0.14	1
ODPB	High side micro	Tyrannosauridae	enamel	12_2	−0.45	0.07	−0.28	0.10	2
ODPB	High side micro	Tyrannosauridae	enamel	12_3	−0.56	0.09	−0.32	0.09	2
ODPB	High side micro	Tyrannosauridae	enamel	12_5	−0.43	0.05	−0.20	0.09	3
ODPB	High side micro	Tyrannosauridae	enamel	12_6	−0.55	0.10	−0.29	0.07	2
ODPB	Tiny horn	Tyrannosauridae	enamel	9_1	−0.49	0.08	−0.25	0.11	2
UMO	Osteolicious	Ceratopsidae	enamel	11_3	−0.86	0.20	−0.51	0.15	3
UMO	Osteolicious	Tyrannosauridae	enamel	11_1	−0.65	0.05	−0.31	0.08	1
UMO	Osteolicious	Tyrannosauridae	enamel	11_2	−0.42	0.07	−0.22	0.10	2
UO	Awesome micro	Ceratopsidae	enamel	10_1	0.05	0.21	0.17	0.21	2
UO	Awesome micro	Ceratopsidae	enamel	10_3	−0.58	0.10	−0.31	0.06	2
UO	Awesome micro	Ceratopsidae	enamel	10_7	−0.39	0.05	−0.25	0.08	2
UO	Awesome micro	Ceratopsidae	enamel	10_8	−0.46	0.10	−0.28	0.14	2
UO	Awesome micro	Ceratopsidae	enamel	10_9	−0.05	0.09	−0.05	0.09	2
UO	Awesome micro	Tyrannosauridae	enamel	10_2	−0.86	0.08	−0.44	0.08	2
UO	Awesome micro	Tyrannosauridae	enamel	10_4	−0.72	0.04	−0.46	0.08	1
UO	Awesome micro	Tyrannosauridae	enamel	10_5	−0.35	0.04	−0.20	0.09	1
UO	Awesome micro	Tyrannosauridae	enamel	10_6	−0.64	0.06	−0.36	0.09	2
UO	Awesome micro	Tyrannosauridae	enamel	10_10	−0.35	0.03	−0.13	0.11	1
UO	Duff micro	Tyrannosauridae	enamel	7_2	−0.77	0.12	−0.44	0.14	2
UO	Jack ceratopsid	Tyrannosauridae	enamel	3_2	−0.56	0.08	−0.38	0.15	2
UO	Last call micro	Ceratopsidae	enamel	15_5	0.05	0.06	−0.03	0.08	2
UO	Last call micro	Ceratopsidae	enamel	15_6	−0.14	0.04	−0.14	0.11	1
UO	Last call micro	Ceratopsidae	dentine	15_6	−0.04	0.05	0.03	0.10	2
UO	Last call micro	Tyrannosauridae	enamel	15_1	−0.63	0.10	−0.30	0.10	3
UO	Last call micro	Tyrannosauridae	dentine	15_1	−0.21	0.05	−0.09	0.12	2
UO	Last call micro	Tyrannosauridae	enamel	15_2	−0.81	0.09	−0.42	0.11	3
UO	Last call micro	Tyrannosauridae	enamel	15_3	−0.67	0.03	−0.30	0.08	1
UO	Last call micro	Tyrannosauridae	enamel	15_4	−0.66	0.05	−0.38	0.09	1
UO	Last call micro	Tyrannosauridae	enamel	15_7	−0.98	0.12	−0.52	0.09	2
UO	Long lag	Ceratopsidae	enamel	6_1	0.38	0.25	0.17	0.28	2
UO	Long lag	Tyrannosauridae	enamel	6_2	−0.81	0.08	−0.48	0.12	2

terrestrial ecosystems of North America and Asia during the Late Cretaceous (Dodson et al., 2004; Sampson et al., 2010; Xu et al., 2010; Lyson and Longrich, 2011; Makovicky, 2012; Maiorino et al., 2015). The elongated mandible of ceratopsids is characterized by an extremely specialized sturdy, toothless and keen-edged beak, that was most likely used to securely grasp and vigorously uproot plants from the soil (Ostrom, 1966; Dodson et al., 2004; Maiorino et al., 2015). These megaherbivores used to consume copious amounts of tough plant material, as suggested by their dentition composed of “Y” shaped teeth, forming complex dental batteries that worked together producing strong shearing forces (Mallon and Anderson, 2014, 2015; Maiorino et al., 2015).

The sample analyzed in this study consists of dinosaur tooth fragments (n = 53) belonging to indeterminate species of tyrannosaurids (n = 29) and ceratopsids (n = 24). They derive from n = 15 different microsites located in Cottonwood Coulee, Fresno Reservoir, near Havre (Montana, USA; Fig. 1, decimal degrees: lat. 48.69, long. −110.01), a small area of US public lands administered by the US Bureau of Land Management. The sample size per taxon for each microsite for tyrannosaurids (T) and ceratopsids (C), are respectively: Bullet micro T = 3, C = 2, Denver side micro T = 2, C = 2, Jack’s bonebed T = 3, C = 1, Jack’s side micro C = 4, Last side micro T = 1, C = 1, Nanoraptor micro C = 4, All crew micro T = 2, C = 1, High side micro T = 4, C = 2, Tiny horn T = 1, Osteolicious T = 2, C = 1, Awesome micro T = 5, C = 5, Duff micro T = 1, Jack ceratopsid T = 1, Last call micro T = 6, C = 3, Long lag T = 1, C = 1. For individual records regarding tissue per taxon for each microsite please refer to Table 1. All the microsites are located within 2 km of each other and document a restricted time frame from the uppermost ~10 m of the Oldman Formation equivalent through the lower ~10 m of the immediately overlying Dinosaur Park Formation. Not all of the samples were analyzed for each geochemical tracer. This is mainly due to the limited sample size and the nature of the performed destructive analyses. Priority was given to Ca isotope analyses (performed on all the samples). Sr and trace elements were performed opportunistically on subsets of samples (see below).

4. Methods

4.1. Trace elements

Trace element concentrations were analyzed *in situ* on a subsample set of n = 15 previously cut and polished teeth (containing 5 dentine and 5 enamel samples for ceratopsids and 2 dentine and 3 enamel samples for tyrannosaurids) with the Thermo Fisher Scientific ICP-MS X series II equipped with the 213 nm laser ablation device UP-213 from New Wave Research housed at the Centro Interdipartimentale Grandi Strumenti (CIGS-UNIMORE; Nardelli et al., 2016; Giovanardi et al., 2018; Medici et al., 2021). The reduced subsample set prioritized well preserved tyrannosaurid and ceratopsian teeth, focusing on macroscopically more intact specimens and paired dentine-enamel samples from the same microsite. As a result, caution is warranted when generalizing the results and the predicted diagenetic trends to the entire fossil collection.

Before optimizing laser ablation for the bioapatite matrix, the instrument was tuned using the NIST 610 and NIST 612 glasses measuring, under optimized working conditions, the intensity of U and Th signals (^{238}U/^{232}Th *vs* ^{238}U). Oxide production was kept below 1 %. To clean up the samples’ surface, a pre-ablation protocol was employed, which consisted of a mild ablation carried out with a fluence that is about 1/10 of the operating conditions. The pre-ablation parameters are: 65 μm of spot-size; 3 J/cm^2; 10 Hz frequency; 5 s of dwell time; 600 ml/min of He flux. Both enamel and dentine were sampled with 55 μm size spots. The laser beam with a fluency varying between 8.5 J/cm^2 and 9.5 J/cm^2 and a frequency of 10 Hz, was used for 45 s on each spot (+15 s of gas blank). Each dental tissue was analyzed (after sampling for isotope analyses) with at least n = 3 spots, performed close to the isotope sampling area. The following isotopes were collected: ^{7}Li, ^{11}B, ^{24}Mg, ^{43}Ca, ^{55}Mn, ^{57}Fe, ^{65}Cu, ^{66}Zn, ^{85}Rb, ^{88}Sr, ^{89}Y, ^{138}Ba, ^{139}La, ^{140}Ce, ^{141}Pr, ^{146}Nd, ^{147}Sm, ^{153}Eu, ^{157}Gd, ^{159}Tb, ^{163}Dy, ^{165}Ho, ^{166}Er, ^{169}Tm, ^{172}Yb, ^{175}Lu, ^{208}Pb, ^{232}Th, ^{238}U. Data reduction was performed following Longerich et al. (1996), using NIST 612 as external reference material and Ca (37 % m/m) as internal standard. The repeatability (% RSD) of the LA-ICP-MS measurements is about 5 % as determined from the analyses of NIST SRM 612 glass. The analytical precision in samples is generally between 5 and 20 % depending on sample inhomogeneities and the elemental concentration of the analyte. NIST-SRM 1400 and NFHS-2-NP (Boer et al., 2022) were measured within the session as quality control reference materials.

4.2. Ca and Sr isotopes

Ca isotopes were measured at the Institute of Geosciences at the University of Mainz (Germany). Enamel and dentine were sampled using a handheld microdrill with a diamond-studded drill bit, carefully separating 0.1 to 1 mg of enamel from the dentine, which was also sampled in similar amounts. For Sr isotopes, the analyzed samples were selected based on the availability of sufficient enamel. In some cases, tooth fragments lacked adequate enamel to be sampled in the desired amounts. Sr isotopes were measured only in those samples where it was possible to sample more than ca. 0.5 mg of enamel. The selection criteria mirrored those used for trace elements (prioritizing macroscopically well preserved samples and, when possible, dentine-enamel pairs per microsite). Samples were then dissolved, digested, and purified in a clean laboratory. No weak acid pretreatment was performed on the samples. First, the sample powder was weighed into Teflon beakers and dissolved in 0.5 mL of concentrated distilled HNO_3. The beakers were then sealed, heated, and evaporated to dryness at 120 °C on a hotplate for 3–5h, the material was then further dissolved in 2 mL 2 N HNO_3. The solution was purified by using a prep*FAST* MC (ESI Elemental Scientific) equipped with a 1 mL Sr-Ca ion chromatographic column following the default Ca separation protocol (Weber et al., 2021). After purification, Ca fractions were evaporated to dryness and distilled conc. HNO_3 and conc. H_2O_2 were added to eliminate potential resin remains. Samples were evaporated to dryness again and dissolved in 0.5 N HNO_3 for analysis.

Samples were analyzed using a Neptune Plus Multicollector-Inductively Coupled Plasma Mass Spectrometer (MC-ICPMS). Sample introduction was performed in 0.5 N HNO_3 using an Apex Omega HF (ESI Elemental Scientific) desolvator system. A standard – sample bracketing approach was applied using an Alfa Aesar plasma standard solution as internal bracketing Ca isotope standard. All solutions were prepared for a 2 mg/L Ca concentration (Weber et al., 2021). Natural Ca isotope abundance ratios exhibit rather modest variations due to the minor fractionation effects in alkali earth elements, therefore the measured Ca isotope compositions must be expressed using the delta (δ) notation:

$$\delta^{44/42}\text{Ca} = (((^{44}\text{Ca}/^{42}\text{Ca})_{\text{sample}}/(^{44}\text{Ca}/^{42}\text{Ca})_{\text{NIST915a}}) - 1) \times 1000$$

where $(^{44}\text{Ca}/^{42}\text{Ca})_{\text{sample}}$ and $(^{44}\text{Ca}/^{42}\text{Ca})_{915a}$ are the Ca isotope abundance ratios measured in the sample and in the NIST SRM 915a standard reference material, respectively. The $\delta^{44/42}$Ca values measured against the in-house standard were converted to NIST SRM 915a following Weber et al. (2021). NIST-SRM 1400 (Bone Ash) was measured (n = 2) as quality control reference material and processed along with the samples, yielding $\delta^{44/42}$Ca values of −0.51 ‰ (± 0.02 ‰, 2SE) and −0.46 ‰ (± 0.01 ‰, 2SE), in agreement with literature data (e.g. −0.54 ‰ ± 0.05 ‰ 2SD, Romaniello et al., 2015; see also Weber et al., 2025).

All Ca isotope literature values are expressed as $\delta^{44/42}$Ca relative to a NIST SRM 915a standard reference material. Data expressed as $\delta^{44/40}$Ca were converted dividing each value by a factor of 2.048 (Martin et al., 2018). Those expressed relative to ICP Ca Lyon standard reference material were converted to NIST SRM 915a by adding 0.52 ‰ (Martin et al., 2015; Balter et al., 2019). The mass-dependent fractionation relationship of the samples measured follows the expected relation for Ca isotopes (see Suppl. Fig. S1).

Sr isotopes were measured at CIGS-UNIMORE following published protocols (see Lugli et al., 2018; Argentino et al., 2021). Sr solutions from the prep*FAST* separation were diluted to 50 ppb with 4 % nitric acid and analyzed through a Neptune MC-ICPMS, housed at the CIGS. Selected samples were also measured for their $\delta^{88/86}$Sr value. Both δ^{88}Sr/^{86}Sr and ^{87}Sr/^{86}Sr were measured within the same analytical session, using the same Sr aliquot. To correct the $\delta^{88/86}$Sr values for mass bias fractionation, samples were spiked with Zr and normalized to the NIST SRM 987 by bracketing (see Argentino et al., 2021). All $\delta^{88/86}$Sr were then expressed relative to NIST SRM 987. Repeated analyses of NIST SRM 987 provided an average ^{87}Sr/^{86}Sr of 0.710262 ± 0.000018 (2 SD, n = 9). Sample ^{87}Sr/^{86}Sr ratios were normalized to a NIST SRM 987 value of 0.710248 (McArthur et al., 2001). The observed reproducibility (2 SD) of the NIST SRM 987 $\delta^{88/86}$Sr was 0.047 ‰ (n = 9). Quality control NIST-SRM 1400 (Bone Ash) yielded $\delta^{88/86}$Sr values of −0.33 ‰ (± 0.03 ‰, 2 SE) and −0.37 ‰ (± 0.04 ‰, 2 SE), in agreement with literature data (e.g. −0.32 ‰ ± 0.03 ‰ 2SD, Romaniello et al., 2015).

5. Results

5.1. Trace elements

The trace element content of tyrannosaurids and ceratopsids are reported in Suppl. Table S1 grouped by taxonomy and dental tissue. The majority of trace elements are more enriched in our samples than in reference values for modern mammal teeth (Kohn et al., 1999, 2013), with few exceptions: Mg is less enriched in both taxa, while Cu and Zn are less enriched in tyrannosaurids (Fig. 2). Yet, modern crocodile data show elemental content of Mg, Fe and Mn closer to our fossil data (Bocherens et al., 1994). Enamel is generally less enriched in diagenetic elements than dentine and this difference is larger in tyrannosaurids than in ceratopsids (Fig. 2).

Enamel total REE abundances (∑REE) are over 1–2 orders higher and more variable in ceratopsids (963 µg/g to 10003 µg/g) than in tyrannosaurids (5.50 µg/g to 56.9 µg/g). Dentine ∑REE values for ceratopsids (3551 µg/g to 19781 µg/g) also reach much higher values than in tyrannosaurids (759 to 1205 µg/g) and are always higher than the enamel ∑REE values for both taxa (Fig. 3; average relative dentine-enamel difference in ceratopsid = 160 % and in tyrannosaurids = 4000 %). Most of the normalized REE profiles of both enamel and dentine have similar patterns with LREE convex downward and MREE to HREE convex upward (Fig. 3), however, enrichments are quite different when considering taxon and tissue. REE enrichment in dentine of ceratopsids is slightly higher than in dentine of tyrannosaurids. Dentine of ceratopsids is slightly more enriched in MREEs than in their enamel. On the contrary, the enamel of tyrannosaurids is much more depleted in all REEs compared to their dentine. One of the most depleted tyrannosaurid enamel patterns (sample 9_1) and one dentine pattern (sample 15_1) show a peculiar HREE enrichment (Fig. 3).

The U content in both dental tissues shows extreme variability with abundances ranging between 0.05 µg/g (min value across both taxa) and 118.32 µg/g (max value across both taxa). Notably, the U content of tyrannosaurids ranges between 0.05 µg/g and 0.24 µg/g, with an average of 0.12 ± 0.10 µg/g (n = 3, SD) for enamel, and between 3.44 µg/g and 14.09 µg/g, with an average of 8.77 ± 7.53 µg/g (n = 2, SD) for dentine. Ceratopsid enamel reaches values between 3.78 µg/g and 35.66 µg/g, with an average of 14.5 ± 13.4 µg/g (n = 5, SD), while dentine ranges between 51.34 µg/g and 118.32 µg/g, with an average of 55.4 ± 40.3 µg/g (n = 5, SD) (Fig. 2, average relative dentine-enamel difference in ceratopsid = 280 % and in tyrannosaurids = 7200 %).

Ce/Ce*, Eu/Eu* and Pr/Pr* values were calculated as Ce/Ce*=2Ce$_N$/(La$_N$ + Pr$_N$), Eu/Eu*=2Eu$_N$/(Sm$_N$ + Gd$_N$) and Pr/Pr*=2Pr$_N$/(Ce$_N$ + Nd$_N$) (Herwartz et al., 2013; Kowal-Linka et al., 2014). Ce/Ce* ranges from 0.59 to 1.04 (mean 0.89 ± 0.12, n = 15, SD), Pr/Pr* from 0.90 to 1.36 (mean 1.01 ± 0.11, n = 15, SD) and Eu/Eu* from 1.08 to 2.26 (mean 1.39 ± 0.34, n = 15, SD). In the plot of Ce/Ce* *vs* Pr/Pr*, a few samples fall in or near the field I, representing samples with neither Ce nor La anomaly. Most samples form a positive trend from field IIa (positive La anomaly, no Ce anomaly) towards lower Ce/Ce* and Pr/Pr* values (Suppl. Fig. S2). Notably, Tyrannosauridae enamel samples plot within the IIIb field (Kowal-Linka et al., 2014), indicative of a true

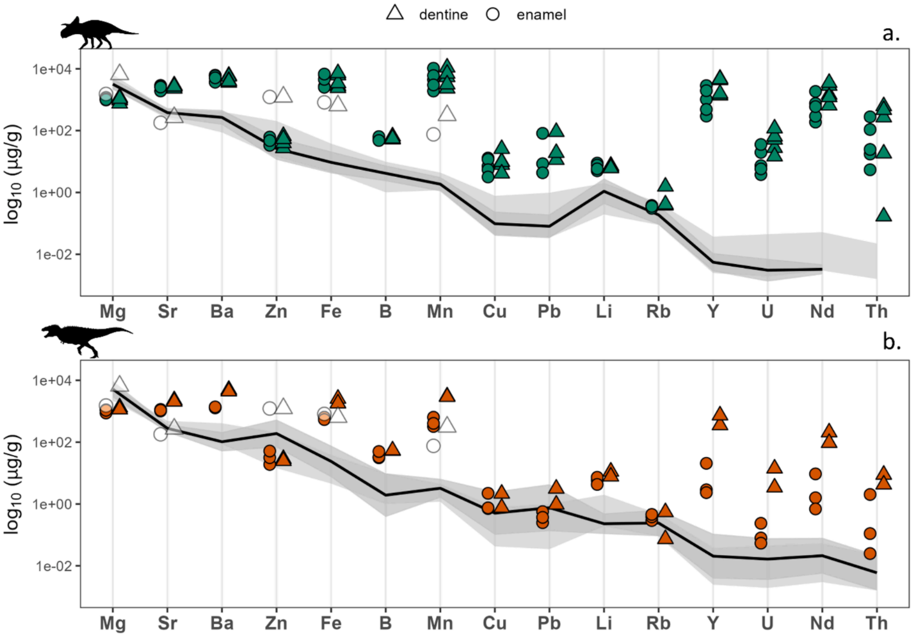

Fig. 2. Trace element data for Ceratopsidae (a.) and Tyrannosauridae (b.). Data are presented as log$_{10}$ µg/g. Light gray ribbons are the overall SD intervals of data for modern mammalian tooth enamel from Kohn et al. (2013), while black lines and dark gray ribbons are mean ± SD of herbivores (in a) and carnivores (in b) from Kohn et al. (2013); empty symbols represent modern crocodile enamel and dentine data from Bocherens et al. (1994). Black silhouettes are from phylopic.org/.

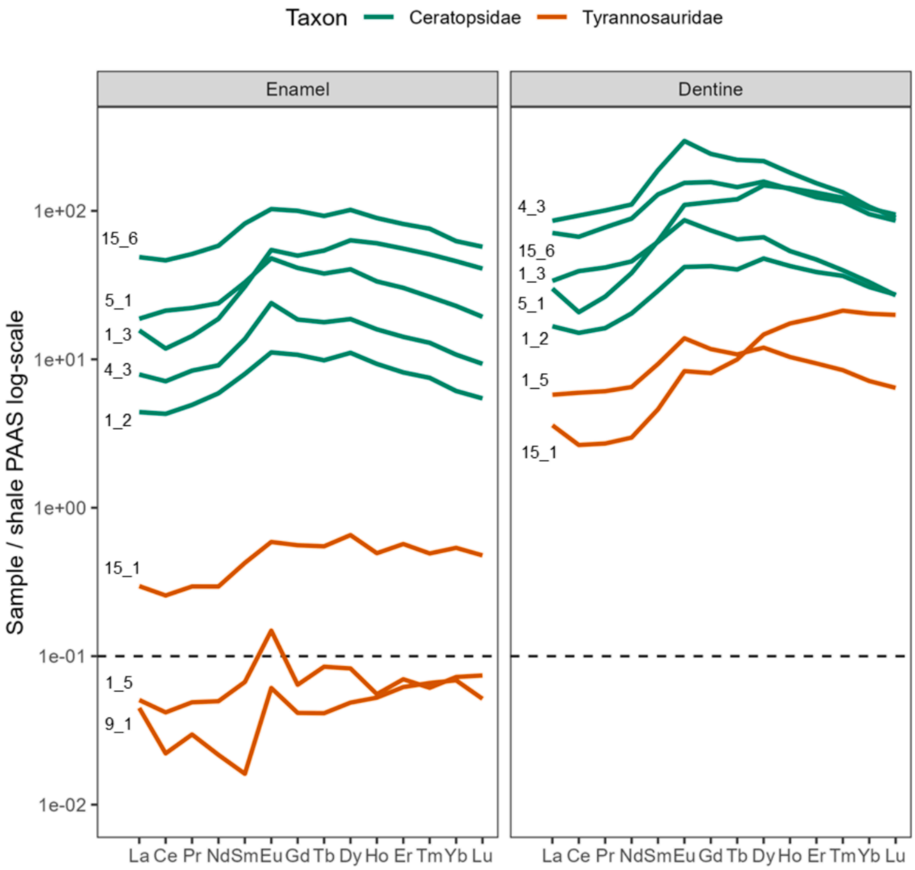

Fig. 3. Comparison of enamel and dentine rare earth elements (REEs) profiles in tyrannosaurid and ceratopsid teeth. The REEs concentration values, expressed in logarithmic scale, are normalized to the Post Archean Australian Shale (PAAS). Intermediate REEs enrichment is greater in ceratopsid enamel and dentine compared to tyrannosaurids. REE concentrations of both ceratopsid dental tissues are not significantly different. Note, modern teeth commonly show total REE contents below ~0.1 μg/g (dashed black line).

negative Ce anomaly. La_N/Yb_N and La_N/Sm_N ratios (Suppl. Fig. S3) show a subvertical trend and are comparable with values for freshwater (Elderfield et al., 1990; Giblin and Dickson, 1992; Johannesson and Lyons, 1995), and for Quaternary sea fish (Elderfield and Pagett, 1986). Notably, one tyrannosaurid dentine is shifted below the values of seawater and one tyrannosaurid enamel is shifted towards those found in Jurassic-Neogene marine fish (Grandjean et al., 1988; Grandjean, 1989; Grandjean and Albarède, 1989). One ceratopsid enamel and one dentine plot between freshwater and seawater values.

5.2. Ca and Sr isotopes

The Ca and Sr isotope compositions are reported in Tables 1–3, grouped by locality and taxon; all values are expressed relative to NIST SRM 915a. The $\delta^{44/42}$Ca was measured mostly in enamel ($n = 53$) and a few dentine samples ($n = 6$). Ceratopsid enamel values are significantly isotopically heavier than those of tyrannosaurids (Wilcoxon rank-sum test, $W = 571$, $p = 3.2e{-}05$; Fig. 4). Ceratopsid $\delta^{44/42}$Ca enamel ranges from −0.86 ‰ to +0.38 ‰ (mean = −0.25 ‰ ± 0.58 ‰, 2SD, n = 24) while that of tyrannosaurids from −0.98 ‰ to −0.26 ‰ (mean = −0.57 ‰ ± 0.36 ‰, 2SD, n = 29). As for dentine, $\delta^{44/42}$Ca values vary between −0.15 ‰ and −0.04 ‰ (mean = −0.09 ‰ ± 0.11 ‰, 2SD, n = 3) for ceratopsids, and between −0.21 ‰ and −0.10 ‰ (mean = −0.14 ‰ ± 0.12 ‰, 2SD, n = 3) for tyrannosaurids.

The intra-site difference (Fig. 5) between carnivores and herbivores ($\Delta^{44/42}Ca_{carnivore\text{-}herbivore}$) ranges from −1.19 ‰ in the “Long Lag” microsite (Upper Oldman Formation) up to 0.33 ‰ in the “Osteolicious” (Uppermost Oldman Formation) microsite (the only positive value). Considering all sites, the average carnivore-herbivore $\delta^{44/42}$Ca offset (considering only enamel values) is −0.29 ‰ ± 0.82 ‰ (2SD, n = 10 microsites with both carnivores and herbivores) (Fig. 5).

Table 2
Strontium isotope ($^{87}Sr/^{86}Sr$) ratios of tyrannosaurid and ceratopsid teeth.

Taxon	Sample	Tissue	$^{87}Sr/^{86}Sr$	2 SE
Ceratopsidae				
	1_2	enamel	0.70821	0.00002
	13_2	enamel	0.70832	0.00002
	5_2	enamel	0.70844	0.00003
	5_2	dentine	0.70828	0.00002
	14_1	enamel	0.70803	0.00002
	10_3	enamel	0.70819	0.00002
	10_7	enamel	0.70838	0.00002
	10_9	enamel	0.70876	0.00002
	15_6	enamel	0.70870	0.00002
	15_6	dentine	0.70863	0.00002
	4_3	dentine	0.70860	0.00002
Tyrannosauridae				
	1_1	enamel	0.70891	0.00002
	13_1	enamel	0.70842	0.00002
	13_1	dentine	0.70808	0.00002
	8_2	enamel	0.70785	0.00003
	14_3	enamel	0.70856	0.00002
	14_3	dentine	0.70793	0.00002
	11_1	enamel	0.70863	0.00003
	10_10	enamel	0.70890	0.00004
	10_4	enamel	0.70873	0.00002
	10_5	enamel	0.70887	0.00002
	15_4	enamel	0.70907	0.00003
	15_1	dentine	0.70812	0.00002

Grouping microsites according to their stratigraphic position yields average $\delta^{44/42}$Ca enamel values for the Upper Oldman Formation of

Table 3
The $\delta^{88/86}$Sr values (relative to NIST 987) of tyrannosaurid and ceratopsid teeth. Samples were not replicated (i.e. n = 1).

Taxon	Sample	Tissue	$\delta^{88/86}$Sr (‰)	2 SE (‰)
Ceratopsidae				
	1_2	enamel	0.26	0.03
	13_2	enamel	0.18	0.03
	5_2	enamel	0.19	0.03
	5_2	dentine	0.34	0.03
	4_3	dentine	0.38	0.03
Tyrannosauridae				
	1_1	enamel	0.14	0.03
	13_1	enamel	0.18	0.03
	8_2	enamel	0.13	0.03
	14_3	enamel	0.30	0.03
	14_3	dentine	0.30	0.03
	11_1	enamel	0.15	0.03
	10_4	enamel	0.03	0.03
	10_5	enamel	0.17	0.03
	10_10	enamel	0.17	0.03
	15_4	enamel	0.02	0.03

−0.14 ‰ ± 0.64 ‰ for ceratopsids (2SD, n = 8) and −0.68 ‰ ± 0.37 ‰ for tyrannosaurids (2SD, n = 13). In the uppermost Oldman Formation values are −0.86 ‰ for ceratopsids (n = 1) and −0.54 ‰ ± 0.33 ‰ for tyrannosaurids (2SD, n = 2). In the Lower Dinosaur Park Formation values are −0.29 ‰ ± 0.52 ‰ for ceratopsids (2SD, n = 12) and −0.47 ‰ ± 0.27 ‰ for tyrannosaurids (2SD, n = 8). Samples with uncertain attribution along the Oldman/Dinosaur Park Formation boundary are on average −0.17 ‰ ± 0.09 ‰ for ceratopsids (2SD, n = 3) and −0.46 ‰ ± 0.22 ‰ (2SD, n = 6) for tyrannosaurids. Enamel and dentine $\delta^{44/42}$Ca pairs from the same dinosaur tooth positively correlate ($R^2 = 0.88$, $p = 0.006$) and show an average dentine-enamel offset of 0.24 ‰ ± 0.15 ‰ (Fig. 6).

Sr isotopes were measured on a smaller subset of samples, mainly due to insufficient material (i.e. small and fragmented samples). The ^{87}Sr/^{86}Sr ratios vary from 0.70793 to 0.70863 in dentine and from 0.70785 to 0.70907 in enamel (Fig. 7). Tyrannosaurid ^{87}Sr/^{86}Sr values for dentine (mean = 0.70803 ± 0.00023, 2SD, n = 3) are on average remarkably lower than those of enamel (mean = 0.70867 ± 0.00071, 2SD, n = 9). Ceratopsid teeth have instead similar values for dentine (mean = 0.70850 ± 0.00035, 2SD, n = 3) and enamel (mean = 0.70838 ± 0.00053, 2SD, n = 8). Enamel values of tyrannosaurids and ceratopsids are statistically indistinguishable (Wilcoxon rank-sum test, W = 16.5, p = 0.066).

The $\delta^{88/86}$Sr values (all expressed relative to the NIST SRM 987) range between 0.02 ‰ and 0.38 ‰, with dentine values all being higher than 0.30 ‰. Ceratopsid $\delta^{88/86}$Sr values range from 0.34 ‰ to 0.38 ‰ for dentine (mean = 0.36 ‰ ± 0.06 ‰, 2SD, n = 2), and from 0.18 ‰ to 0.26 ‰ for enamel (mean = 0.21 ‰ ± 0.09 ‰, 2SD, n = 3). Tyrannosaurid teeth display a value of 0.30 ‰ for dentine and range from 0.02 ‰ to 0.30 ‰ (mean = 0.14 ‰ ± 0.16 ‰, 2SD, n = 9) for enamel. The average (enamel) difference between carnivore and herbivore $\delta^{88/86}$Sr values is only −0.07 ‰, and is not statistically significant (Wilcoxon rank-sum test, W = 23, p-value = 0.1).

Due to the limited number of specimens measured for Sr, the comparison among micro-sites is not significant. For this reason, we decided to focus our evaluations of the Sr dataset as a whole rather than dividing it among micro-sites/stratigraphic units, as was done for Ca isotopes. However, Fig. 7 reports radiogenic Sr isotope values organized by micro-site for future reference.

6. Discussion

The assessment of *post mortem*, diagenetically induced chemical alteration is critical to define the degree of preservation of biogenic isotopic proxies. In the following section we first evaluate overall diagenetic alteration using trace element geochemistry. We then assess potential dietary information through Ca isotopes, followed by the characterization of biogenic signals using stable Sr isotopes. Finally, we model diagenetic processes by integrating stable Ca-Sr isotope data with radiogenic Sr isotope ratios to effectively disentangle biogenic from geogenic signals. We conclude by highlighting the geochemical significance and broader implications of our findings, and recommend analysing the stable $\delta^{88/86}$Sr ratio alongside the traditional ^{87}Sr/^{86}Sr in fossil specimens, to better assess the pathways of Sr diagenetic alteration.

6.1. Diagenesis

The trace element contents in dentine and enamel of our (sub)samples show typical enrichments compared to modern mammal teeth, likely related to diagenetic processes (see e.g., Fe, Mn, REEY and U in Fig. 2). Similarly, Mn and Sr are more enriched in our samples compared

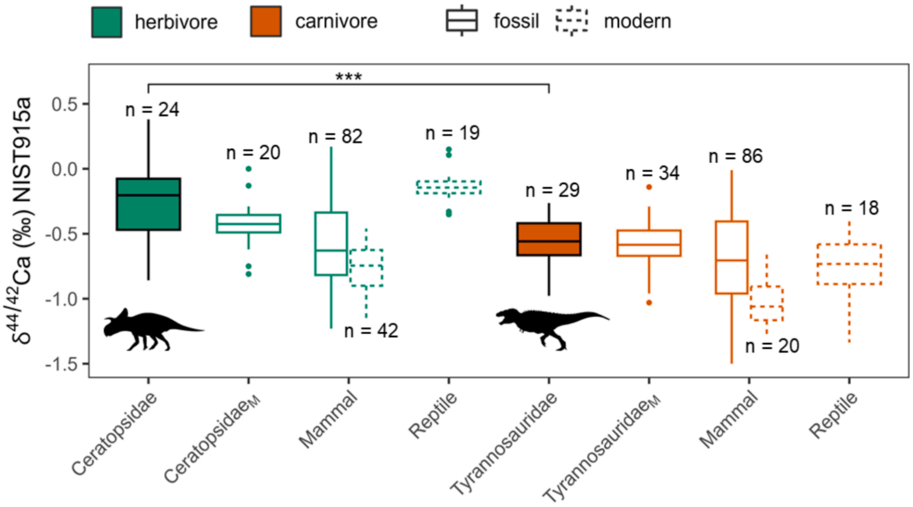

Fig. 4. Calcium isotope data of the analyzed tyrannosaurid (n = 29) and ceratopsid (n = 24) tooth enamel (filled boxes; *** significant difference through Wilcoxon rank-sum test, W = 571, p = 3.2e−05), compared with Martin et al. (2022) (subscript $_M$) and literature data (empty boxes) of fossil (solid line) and modern (dashed line) enamel $\delta^{44/42}$Ca values for mammal and reptile carnivores and herbivores. All the values are expressed as $\delta^{44/42}$Ca ‰, relative to NIST SRM 915a. Compiled literature data from: Chu et al., 2006; Reynard et al., 2010, 2011; Heuser et al., 2011; Martin et al., 2015, 2017, 2018; Hassler et al., 2018; Guiserix et al., 2024; Weber et al., 2025. The whole dataset, including literature data, is available at: https://zenodo.org/records/15041285.

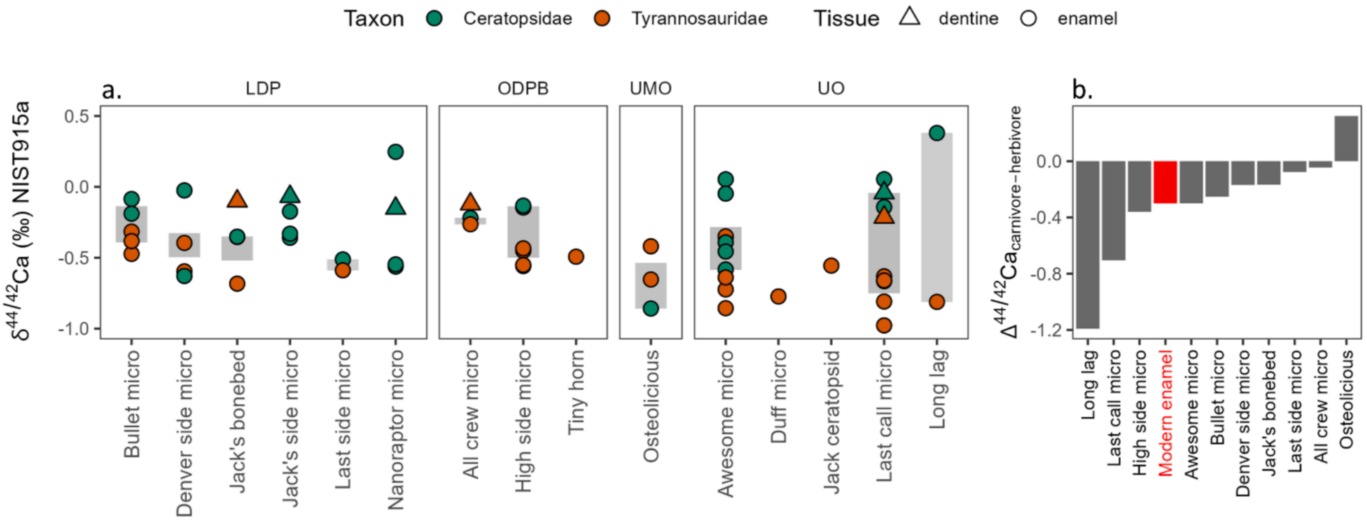

Fig. 5. Calcium enamel isotope variability by stratigraphic position (a.; LDP: Lower Dinosaur Park; ODPB: Oldman/Dinosaur Park boundary; UMO: Uppermost Oldman; UO: Upper Oldman) and microsites of tyrannosaurid (orange) and ceratopsid (green); dentine samples are reported as triangles. All the values are expressed as $\delta^{44/42}$ Ca (‰), relative to the NIST SRM 915a. The differences (delta Δ) between carnivores' and herbivores' average enamel values are represented as gray bars and they are plotted on the right in the $\Delta^{44/42}\text{Ca}_{\text{carnivore-herbivore}}$ diagram (b., ascending order; see text for details); the red bar is a modern enamel dataset of African terrestrial mammals from Martin et al. (2018) as comparison. Sample size per microsite for tyrannosaurids: Bullet micro n = 3 (enamel); Denver side micro n = 2 (enamel); Jack's bonebed enamel n = 1, dentine n = 1; Last side micro n = 1 (enamel); All crew micro enamel n = 1, dentine n = 1; High side micro n = 4 (enamel); Tiny horn T = 1 (enamel); Osteolicious n = 2 (enamel); Awesome micro n = 5 (enamel); Duff micro n = 1 (enamel), Jack ceratopsid n = 1 (enamel), Last call micro enamel n = 5, dentine n = 1; Long lag n = 1 (enamel). Sample size per microsite for ceratopsids: Bullet micro n = 2 (enamel); Denver side micro n = 2 (enamel); Jack's bonebed n = 1 (enamel); Jack's side micro enamel n = 4, dentine n = 1; Last side micro C = 1 (enamel); Nanoraptor micro enamel n = 3, dentine n = 1; All crew micro enamel n = 1, dentine n = 1; High side micro n = 2 (enamel); Osteolicious n = 1 (enamel); Awesome micro n = 5 (enamel); Last call micro enamel n = 2, dentine n = 1; Long lag C = 1 (enamel).

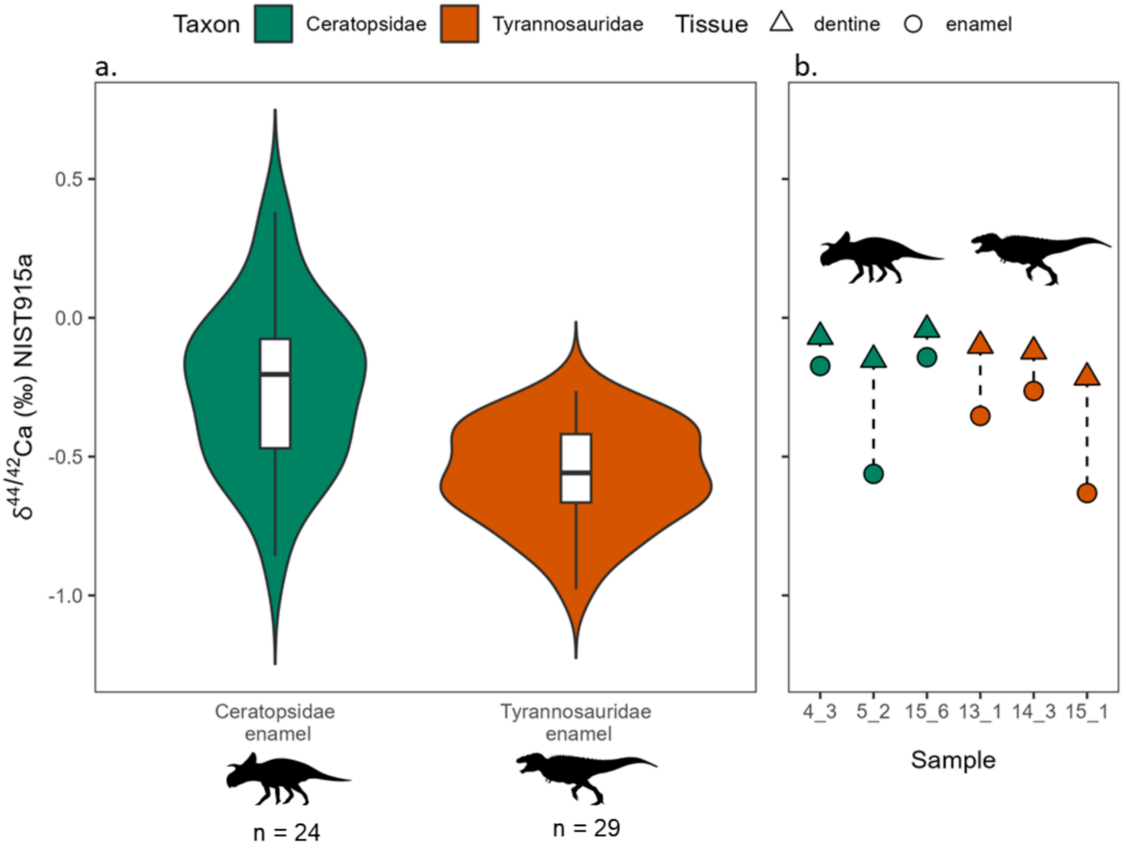

Fig. 6. $\delta^{44/42}$Ca (‰) violin plots (a.) for enamel of the analyzed tyrannosaurid (orange, n = 29) and ceratopsid (green, n = 24) teeth. Although statistically different (see Fig. 4), there is a partial overlap between tyrannosaurid and ceratopsid enamel datasets. Dentine values (reported as triangles) are similar for both taxa (b.) and are always heavier and heavier than their relative enamel value. Black silhouettes are from phylopic.org/.

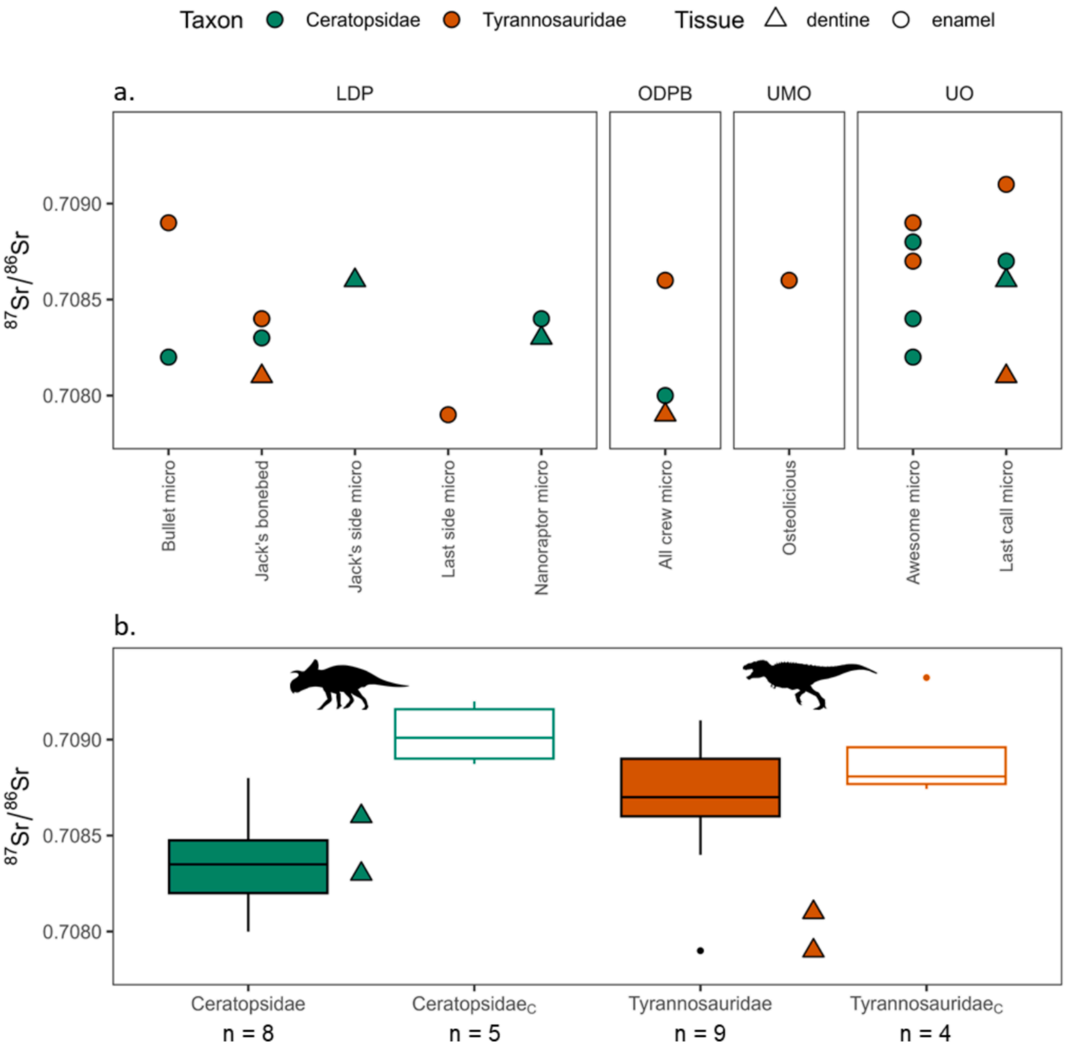

Fig. 7. a. Strontium isotope variability by stratigraphic position (a.; LDP: Lower Dinosaur Park; ODPB: Oldman/Dinosaur Park boundary; UMO: Uppermost Oldman; UO: Upper Oldman) and microsites of tyrannosaurid (orange) and ceratopsid (green); dentine samples are reported as triangles, enamel as circles. Bullet micro, n = 2 (enamel only); Jack's bonebed, enamel n = 2, dentine n = 1; Jack's side micro, n = 1 (dentine only); Last side micro, n = 1 (enamel only); Nanoraptor micro, enamel n = 1, dentine n = 1; All crew micro, enamel n = 2, dentine n = 1; Osteoliscious, n = 1 (enamel only); Awesome micro, n = 5 (enamel only); Last call micro, enamel n = 2, dentine n = 2. b. Enamel $^{87}Sr/^{86}Sr$ isotope data of tyrannosaurids (orange, n = 8) and ceratopsids (green, n = 8) from this study (filled boxes) are compared with enamel data from Cullen et al. (2022) (empty boxes, subscript $_C$); dentine values (tyrannosaurids n = 2, ceratopsids n = 2; this study) are reported as triangles. Marine seawater at 75 Ma is equal to 0.7076 (McArthur et al., 2001).

to modern crocodiles, both these elements are commonly uptaken during diagenetic alteration (Kohn et al., 1999; Nava et al., 2020). Instead, Mg and Zn are depleted (Fig. 2) compared to modern crocodiles and mammals. This could be attributed to the comparatively low Mg and Zn content of soil versus bioapatite (i.e. lack of uptake) and/or to a diagenetic pathway causing potential leaching of those elements from teeth (e.g., Kohn et al., 1999; Nava et al., 2020; Rey et al., 2022). This behavior might support the exploration of Zn and Mg isotope analyses of dinosaur's enamel to further develop the reconstruction of their trophic niches, as already successfully applied for Zn isotopes to Cenozoic fossil teeth (Bourgon et al., 2021; McCormack et al., 2022). Fe – typically enriched in diagenetically altered bioapatite (Kohn et al., 1999) – is higher in ceratopsid teeth (both dentine and enamel) and tyrannosaurid dentine than modern crocodile dental tissues; but it is slightly lower in tyrannosaurid enamel than modern crocodile enamel.

Modern bones and teeth typically contain less than 1 μg/g of total REE (see e.g., Kohn et al., 2013), so the enrichment observed in most of our specimens (Fig. 3) is likely caused by *post mortem* diagenetic uptake. All the analyzed specimens, except tyrannosaurid enamel, show either no or positive Ce anomalies and positive Eu anomalies, suggesting oxidizing conditions during diagenesis. The lower REE contents in tyrannosaurids suggest reduced post-depositional alteration. Most samples show MREE enrichment and a subvertical trend in the La_N/Yb_N versus La_N/Sm_N, suggesting prolonged inorganic REE absorption (Reynard and Balter, 2014; Trueman and Tuross, 2002 and references therein) (Suppl. Fig. S3). Most data for ceratopsids and tyrannosaurids are similar to bioapatite from freshwater settings (Elderfield et al., 1990; Giblin and Dickson, 1992; Johannesson and Lyons, 1995) and suggest that REE fractionation reflects absorption processes or changes in freshwater-seawater mixing over time (Reynard et al., 1999; Reynard and Balter, 2014). In contrast, Cretaceous dinosaur teeth from Alberta (Martin et al., 2022) show lower La_N/Yb_N and La_N/Sm_N values likely due to differences in diagenetic processes or depositional settings (Reynard et al., 1999; Reynard and Balter, 2014).

Variations in U content between enamel and dentine indicate differential diagenetic uptake from ambient pore water, with Tyrannousaurids showing the lowest U content, similar to modern bioapatite (see Results). Uranium, as a water-soluble uranyl ion ($(UO_2)^{2+}$) is highly mobile and rapidly incorporated into bioapatite during (early) diagenesis (Kohn et al., 1999; Gatti et al., 2022; Smedley and Kinniburgh, 2023). Fresh bioapatite typically contains < 1 µg/g U (Kohn et al., 1999), whereas fossil bioapatite often has 10–100 µg/g, making U a sensitive marker to determine post-burial elemental uptake (e.g., Millard and Hedges, 1996; Trueman et al., 2008; Gatti et al., 2022). Variations in U content across sites likely reflect differences in local water U concentrations or flow paths, potentially affecting some sites more than others. Notably, teeth from different taxa show distinct REE and U uptake, despite similar depositional and taphonomic settings.

We propose that differences in enamel microstructure (Sander, 1999; Hwang, 2005, 2011) possibly explain the varying diagenetic alterations observed between tyrannosaurid and ceratopsid teeth. Tyrannosaurid teeth feature a continuous enamel cover (80–200 µm) with thicker enamel on denticle tips and well-developed inner columnar structures with non-exposed tubules (Suppl. Fig. S4-A, B) (Sander, 1999; Hwang, 2005, 2011). In contrast, ceratopsid teeth fragments are covered in enamel on one side only, with a split exterior showing variable thickness (60 to 400 µm) and pervasive tubules throughout (Suppl. Fig. S4-C, D) (Sander, 1999; Hwang, 2005, 2011). We speculate that these differences in tooth morphology and histology (i.e., enamel microstructure and porosity) between the two taxa, might have controlled REE and U uptake, with tyrannosaurid enamel remaining more pristine. This is supported by lower REE and U contents in tyrannosaurids and minimal ^{87}Sr/^{86}Sr differences between ceratopsid enamel (0.7084) and dentine (0.7085), which will be further discussed in the following sections, possibly reflecting more diagenetic alteration in ceratopsid enamel.

6.2. *Ca isotopes as proxy for diet reconstruction*

Although there is a partial overlap in the $\delta^{44/42}$Ca data, the vast majority of ceratopsid enamel values are higher (0.32 ‰ on average) than those of tyrannosaurid enamel values (Fig. 4). The trophic level difference between the two taxa is comparable to previous studies on Jurassic and Cretaceous dinosaurs (among others, tyrannosaurids, ceratopsids, hadrosaurids) species (Heuser et al., 2011; Hassler et al., 2018; Martin et al., 2022). There is no apparent relationship between Ca isotopes and diagenetic markers, supporting the idea of a preservation of the biogenic signal (Fig. 8).

Carnivorous non-spinosaurid theropods from the Gadofauna (Albian/Aptian, Niger) (Hassler et al., 2018, 2021) show enamel $\delta^{44/42}$Ca values comparable to our tyrannosaurids, even if slightly more enriched (−0.75 ‰ to −0.23 ‰, mean = −0.43 ‰ ± 0.32 ‰, 2SD, n = 9). In contrast, herbivorous Iguanodontid (*Ouranosaurus nigeriensis*, an ornithischian dinosaur from the Gadofauna of Niger) (Hassler et al., 2018; mean = −0.04 ‰ ± 0.10 ‰, 2SD, n = 9) display values between −0.14 ‰ and +0.02 ‰, aligning with the upper range of ceratopsid enamel. Additionally, our Tyrannosaurid average (−0.57 ‰ ± 0.36 ‰, n = 29) closely matches the value reported by Martin et al. (2022) (−0.58 ‰ ± 0.36 ‰, 2SD, n = 34), while our ceratopsid data (mean = −0.25 ‰ ± 0.58 ‰, n = 24) lies in between their ceratopsid (−0.8 ‰ to 0.00 ‰, mean = −0.43 ‰ ± 0.36 ‰, 2SD, n = 20) and hadrosaurid (−0.42 ‰ to + 0.42 ‰, mean = −0.14 ‰ ± 0.41 ‰, 2SD, n = 17) values. The $\Delta^{44/42}\text{Ca}_{\text{carnivore-herbivore}}$ offset between the two dinosaur taxa in our dataset is −0.32 ‰, a value consistent with trophic level differences observed in modern and fossil ecosystems (e.g., −0.30 ‰ in African mammals and −0.44 ‰ to −0.79 ‰ in extant reptiles. Fig. 5, data from: Chu et al., 2006; Reynard et al., 2010, 2011; Heuser et al., 2011; Martin et al., 2015, 2017, 2018, 2022; Hassler et al., 2018; Weber et al., 2025). In comparing our dinosaur data with modern mammals and reptiles, both dinosaur taxa exhibit $\delta^{44/42}$Ca that more closely resemble those of reptiles (Fig. 4). In addition, our ceratopsid data overlap with both ceratopsids and hadrosaurids from Martin et al. (2022), thus suggesting that differences in plant consumption were not exclusive to either taxon, with species or genera specific feeding behaviors possibly contributing to the broad observed range of $\delta^{44/42}$Ca values.

Variations in the herbivore-carnivore isotopic offset across formations are notable: the upper Oldman Formation shows an offset of −0.54 ‰, while the Lower Dinosaur Park Formation of −0.18 ‰. This variation may reflect shifts in prey preference/availability and environmental changes across the Judith River-Belly River discontinuity. The vast floodplains of the Oldman Formation with low sinuosity, fast flowing rivers near marine environments likely supported large numbers of ceratopsids, making them the main prey of tyrannosaurids (as evidenced by herbivore-carnivore $\delta^{44/42}$Ca offset of −0.54 ‰). We speculate that the rapid transgression of the Western Interior Seaway restructured alluvial systems, potentially reducing ceratopsid population in the more waterlogged Dinosaur Park Formation and forcing tyrannosaurids, which have no specific habitat preference (Lyson and Longrich, 2011), to diversify their prey. These might include not only ceratopsids and

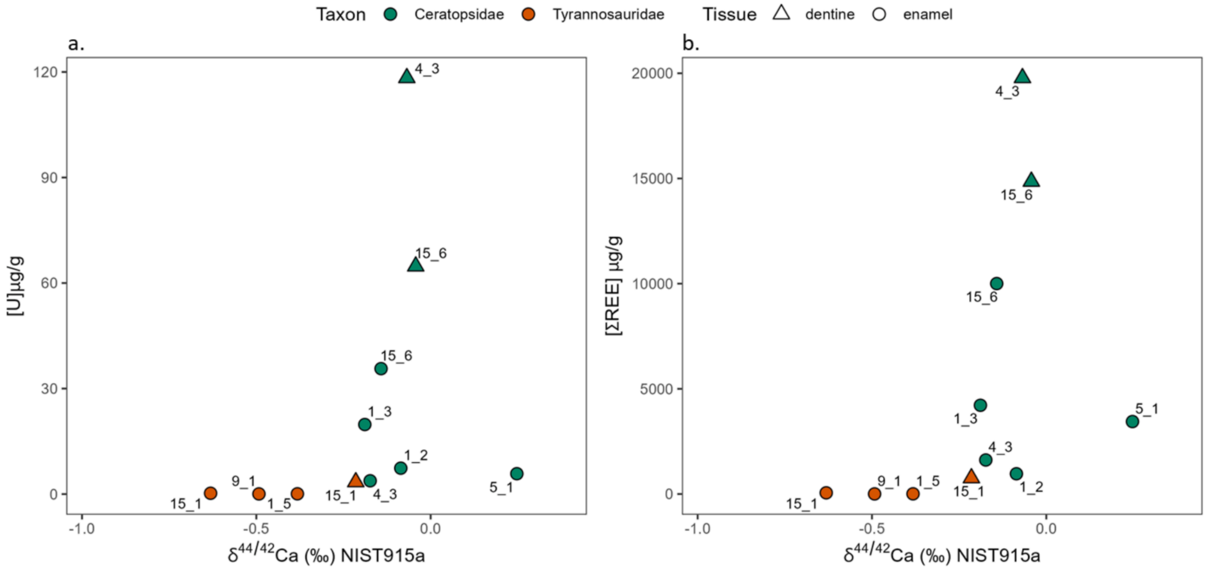

Fig. 8. Calcium isotope variability compared to the content of uranium (a.) and rare earth elements (∑REE, b.) in tyrannosaurid and ceratopsid tooth fragments. The data is shown for dentine (triangles) and enamel (circles). Ceratopsid dentine and enamel have the highest U and REE values. Tyrannosaurid tissues show lower values, with dentine only slightly more enriched than enamel. Note, there is no correlation of diagenesis indicating U and REE with $\delta^{44/42}$Ca, hence Ca isotopes still seem to reflect original diet related values.

hadrosaurids, but also other ornithischian dinosaurs, such as ankylosaurids and pachycephalosaurids, each with potentially distinct food preferences. This is further supported by findings on *Gorgosaurus* stomach contents and its opportunistic consumption of caenagnathids (Therrien et al., 2023). Hadrosaurids might have encountered an increased abundance of low growing vegetation in the vast floodplains of the Oldman Formation, instead of their preferred higher growing plants. This shift could result in hadrosaurids exhibiting $\delta^{44/42}$Ca values more similar to those of ceratopsids, which in turn would affect the isotopic signals in their predators. Additionally, tyrannosaurids are also known for being opportunistic feeders, with cannibalistic tendencies as shown by bite marks on other tyrannosaurid bones (Jacobsen, 1998; Longrich et al., 2010; Martin et al., 2022). Therefore, the systematic variation of tyrannosaurid mean $\delta^{44/42}$Ca values through time (−0.68 ‰ ± 0.37 ‰ in the Oldman Formation, −0.54 ‰ ± 0.33 ‰ in the uppermost Oldman Formation, −0.46 ‰ ± 0.22 ‰ at the Oldman/Dinosaur Park Formation boundary, −0.47 ‰ ± 0.27 ‰ in lower Dinosaur Park Formation) might likely reflect a shift in their diet or in the diet of their prey.

Isotopic variability is further complicated by spatial differences, with enamel $\delta^{44/42}$Ca values varying across the fifteen analyzed microsites (Fig. 5). Tyrannosaurids values are systematically lower than ceratopsids, except at one site (Osteolicious). The largest differences occur at Long lag, Last call micro and High side microsites, however, it remains unclear if these differences reflect spatial variations in ceratopsid diet, prey selection or post burial alteration. Intra-microsite variability in $\delta^{44/42}$Ca values might also be the result of a limited sample size, as only a few of the 15 analyzed microsites (e.g., Bullet micro, High side micro, Awesome micro and Last call micro) contain sufficient samples for robust comparison. Consequently, inter-microsite trends should be interpreted with caution.

The similar average $\delta^{44/42}$Ca values in dentine between herbivores and carnivores (mean difference of −0.06 ‰), and consistently higher dentine $\delta^{44/42}$Ca values compared to enamel, indicate no clear trophic effect is retained in dentine. However, six paired dentine and enamel samples are positively correlated, with dentine being ^{44}Ca-enriched in both taxa. This trend is steeper (slope = 3.09 ± 0.58) than the expected 1:1 line for unaltered tissue (Suppl. Fig. S5). Diagenesis of only dentine tissue would move the line towards more positive x-values maintaining a slope equal to one. This suggests that some diagenetic alteration, particularly in ceratopsid enamel, may affect the magnitude of the trophic signal. Overall, our findings support previous observations that enamel is more resistant to diagenetic alteration than dentine, with tyrannosaurid enamel likely retaining a more pristine elemental/isotopic record signature than that of ceratopsids (Thorp and Vandermerwe, 1987; Ayliffe et al., 1994; Wang and Cerling, 1994; Kohn et al., 1999). Although we cannot exclude that some diagenetic alteration might have occurred, our isotope dataset suggests that the Ca isotopic composition looks unaltered, potentially preserving important biologically derived trophic partitioning between carnivores and herbivores, and possibly hinting at some degree of predator/prey relationship shifting through time. This is of particular importance because having a strong reliable proxy, resistant to chemical alteration, might be useful to infer past vertebrate diet and to assess the reliability of other isotope systematics. In addition, due to the abundance of fossil material of diverse species in the Judith River Formation, future Ca isotopes studies could refine our understanding of tyrannosaurid feeding preferences during the Campanian. A comprehensive study through time might reveal how environmental changes across the Judith River-Belly River discontinuity affected tyrannosaurids' ecology.

6.3. *Diet vs diagenesis – implications from Sr isotopes*

Stable Sr isotopes are increasingly used in dietary studies, because $\delta^{88/86}$Sr values systematically decrease along the food chain (Knudson et al., 2010; Tütken et al., 2015; Guiserix et al., 2024; Weber et al., 2025). In our dinosaur teeth dataset, the average carnivore-herbivore enamel $\delta^{88/86}$Sr offset is −0.07 ‰, smaller than in modern African mammals (~ −0.18 ‰; Tütken et al., 2015) and reptiles (−0.19 ± 0.14 ‰ between herbivores and varanids, −0.18 ± 0.15 ‰ between herbivores and Crocodylia, Weber et al., 2025), as well as in Late Pleistocene mammalian fossils (~ −0.10 ‰, all data from Guiserix et al., 2024; −0.14 ‰, enamel only from Guiserix et al., 2024). While Ca appears as a strong and reliable proxy resistant to post-depositional alterations, this does not appear to be the case for Sr. The smaller observed offset of $\delta^{88/86}$Sr might suggest a possible diagenetic overprint that reduces the stable Sr isotope difference induced by *in vivo* trophic fractionation.

If the biogenic, diet-related Sr isotope composition were fully preserved, we would expect a positive correlation between Ca and stable Sr isotope ratios, as seen in modern mammals and reptiles, which plot on linear regression lines (Tütken et al., 2015; $y = 0.42x - 0.135$; Weber et al., 2025; $y = 0.35x - 0.153$). A recent study by Guiserix et al. (2024) also shows a positive correlation for Middle Paleolithic (ca. 50 ka) herbivores and carnivores from Europe ($y = 0.29x + 0.08$), but with less negative $\delta^{88/86}$Sr values compared to modern bones (Tütken et al., 2015).

Our dinosaur dentine and enamel specimens show a significant positive correlation between $\delta^{44/42}$Ca and $\delta^{88/86}$Sr ($y = 0.41x + 0.35$; $R^2 = 0.76$; $p = 2.4\text{E-}05$), with the highest $\delta^{44/42}$Ca and $\delta^{88/86}$Sr values in dentine (Fig. 9). The data plot on a line with a slope similar to the modern mammal and reptile trophic relationship, but $\delta^{88/86}$Sr values are all positive (i.e., no trophic depletion of ^{88}Sr) and trend towards a theoretical diagenetic $\delta^{88/86}$Sr geogenic end-member of ~0.40 ‰ (see values for e.g., sea-/freshwaters, soils and rocks in Knudson et al., 2010 and reference therein). Altogether, these correlations suggest a similar biological behavior of stable Sr and Ca isotopes, leading to a systematic trophic fractionation (i.e., decreasing $\delta^{88/86}$Sr and $\delta^{44/42}$Ca) along the food chain. In fossils, diagenetic processes may shift these values towards geogenic isotope compositions predominantly affecting Sr, whereas Ca remains largely unaffected due to its high abundance in bioapatite (Heuser et al., 2011; Dodat et al., 2023).

Similar $\delta^{88/86}$Sr in our samples and modern mammals/reptiles (i.e., different species and geographic origins) suggest that fractionation is mainly driven by diet. This, in turn, strongly indicates that such positive values are likely geogenic, thus diagenetically overprinted, or represent a mix of biogenic and geogenic end-members. Starting from the modern reptiles fractionation line (Weber et al., 2025), the addition of different amounts of diagenetic Sr ($\delta^{88/86}$Sr = 0.40 ‰, reflecting the average value of silicate/sedimentary rocks as potential diagenetic endmember of Sr dissolved in sedimentary pore fluids), through a simple mixing model, increases the intercept and lowers the slope of the original diet-related biogenic trend. This is consistent with observations from Middle Paleolithic samples from Guiserix et al. (2024), which plot close to the theoretical line of 40 % diagenetic Sr ($f_{0.4}$), possibly suggesting a partial diagenetic overprint of the $\delta^{88/86}$Sr values; this is also evident when bones-only data are plotted (line a, Fig. 9), showing a smaller slope than enamel-only (line b). Yet, we must point out that these fossils (like ours) originate from environmental, geological and chronological contexts that differ from modern mammals and reptiles of Tütken et al. (2015) and Weber et al. (2025).

The regression line ($y = 0.41x + 0.35$) of our dinosaur data cuts the modeled diagenetic trends and can be approximated by applying a different diagenetic proportion of Sr, with more diagenetic contribution (~85 %) to the specimens with the highest $\delta^{44/42}$Ca (ceratopsid enamel, and dentine of both taxa) and less (~60 %) to those with the lowest $\delta^{44/42}$Ca (tyrannosaurid enamel). This also suggests that diagenesis affects Sr in enamel differently between taxa (i.e., more alteration of the ceratopsid enamel with higher $\delta^{88/86}$Sr and $\delta^{44/42}$Ca), as also observed in trace elements data (see Fig. 2 and Suppl. Fig. S6, where samples with higher Sr content also show higher U and REE contents). Moreover, dentine is overall more affected by diagenesis than enamel.

The relationship observed in Fig. 9, however, may also reflect

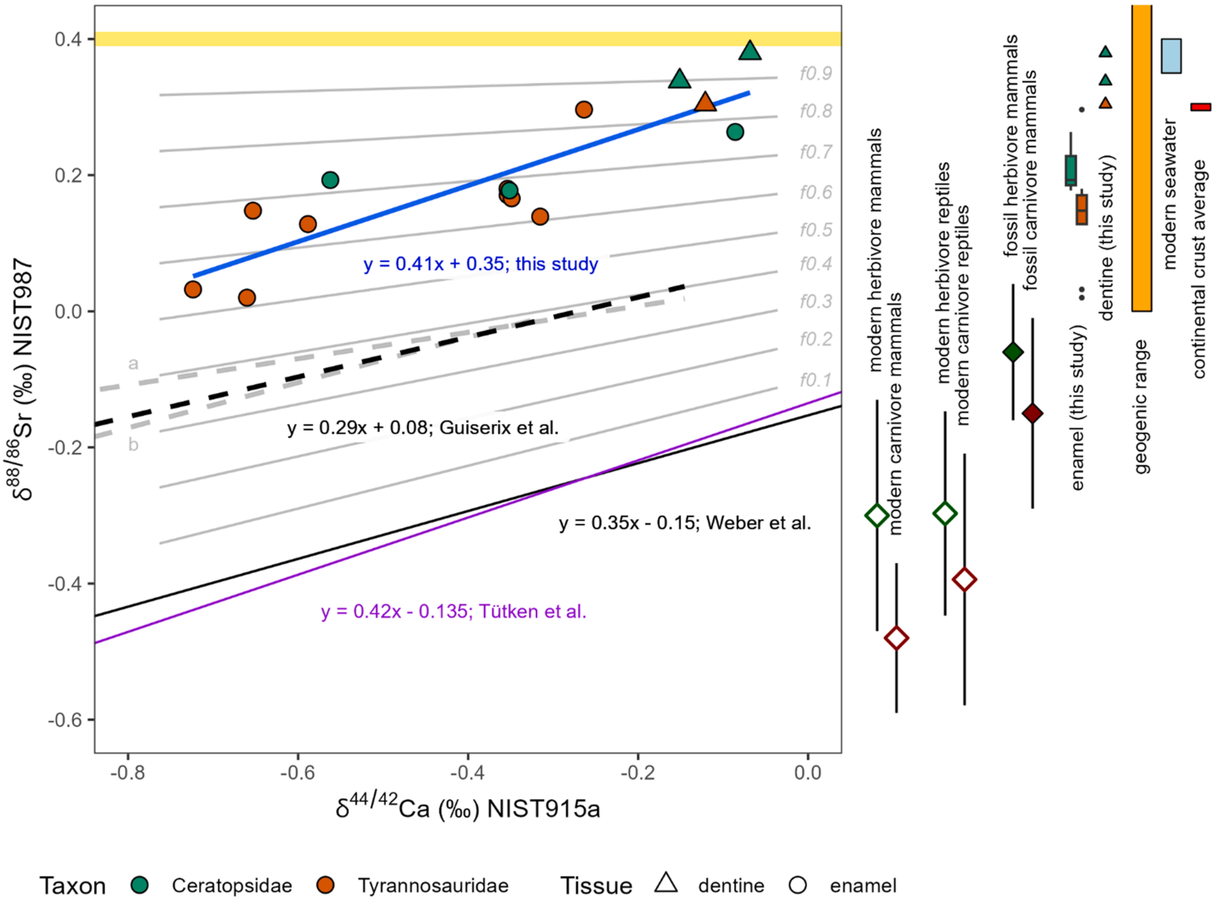

Fig. 9. Correlation plots between $\delta^{44/42}$Ca and $\delta^{88/86}$Sr of dentine (triangles) and enamel (circles) of the analyzed tyrannosaurid (orange) and ceratopsid (green) teeth. The blue line is the linear fit of the data from this study; the purple line is the linear fit of modern African mammals from Tütken et al. (2015); the black line is the linear fit of modern reptiles from Weber et al. (2025); the dashed black line is the linear fit of a fossil European (~50 ka) trophic chain from Guiserix et al. (2024), including both bone and enamel samples; the two dashed gray lines are the linear fits from Guiserix et al. (2024) including bone samples only (a) and enamel samples only (b). Gray lines represent the linear fit of modern reptiles from Weber et al. (2025) with an increasing proportion of diagenetic Sr ($\delta^{88/86}$Sr = 0.40 ‰, see text for details) added to each sample (f_0 = 0 % diagenetic contribution, $f_{0.9}$ = 90 % diagenetic contribution). The yellow line is the diagenetic Sr end-member used in the model. On the right, $\delta^{88/86}$Sr modern data from Tütken et al. (2015; bone samples), modern data from Weber et al. (2025) and fossil data from Guiserix et al. (2024; bone + enamel samples) and our data are reported as comparison. Geogenic (up to ~0.50 ‰) and modern seawater (~0.39 ‰) ranges are also reported (see Hajj et al., 2017); the geogenic range includes also freshwater values (average ~0.32 ‰) which largely overlap with rock values (continental crust average ~0.30 ‰).

diagenetic effects on Ca isotope composition. Given that the stable Sr isotope ratios appear to be altered by post-depositional diagenesis, we cannot completely rule out the possibility that the enamel specimens experienced similar, albeit lesser, alterations due to the inherited resistance of enamel Ca (Heuser et al., 2011; Dodat et al., 2023). Consequently, our interpretation should be treated with caution, acknowledging that limited diagenetic effects might partly account for the observed Ca isotope variability.

To further evaluate diagenetic alteration of Sr in dentine and enamel and to better determine the diagenetic end-member, we examined their ^{87}Sr/^{86}Sr ratios, which commonly represents the (bio)available Sr in the environment. The ^{87}Sr/^{86}Sr of our dinosaur teeth are all more radiogenic than the contemporaneous seawater value (0.7076, from McArthur et al., 2001), representing a potential diagenetic end-member for marine influenced pore water in near-coastal depositional settings. This indicates incorporation of Sr from sedimentary sources, whether *in vivo* (bioavailable Sr from food sources) or *post mortem* (dissolved Sr from ground/pore water). However, our stable Sr *vs* Ca model suggests that only 15 to 40 % of the original biogenic Sr might be retained. This limited retention complicates (paleo)ecological interpretations based on radiogenic Sr isotopes and suggests that the differences observed between tyrannosaurids and ceratopsids likely results from a mix of diagenetic overprint and residual biogenic signal.

A weak negative correlation between $\delta^{88/86}$Sr and ^{87}Sr/^{86}Sr ($R^2 = 0.19, p = 0.11$; Fig. 10), indicates that samples with the highest ^{87}Sr/^{86}Sr and the lowest $\delta^{88/86}$Sr, particularly tyrannosaurid enamel, which also shows the lowest $\delta^{44/42}$Ca values, may retain a small portion of their original biogenic Sr signal (both stable and radiogenic). In contrast, ceratopsid enamel and dentine, along with tyrannosaurids dentine, tend towards a less radiogenic end-member (possibly seawater), suggesting poorer preservation in these tissues.

The enamel Sr isotope ratios of Late Cretaceous tyrannosaurids and ceratopsids of the upper Oldman Formation in Canada (Cullen et al., 2022; note that their samples have been leached with acetic acid prior dissolution) overlap and are overall higher than those in our dataset (Fig. 7). Although both studies are stratigraphically correlated, differences in proximity to the Western Interior Seaway led to varying terrigenous versus marine Sr influences. Cullen et al. (2022) observed significant dispersion in tyrannosaurid Sr isotope ratios (SD = 0.00027), which may indicate high mobility across regions with varying bedrock ^{87}Sr/^{86}Sr signatures or a mix of biogenic and diagenetic Sr. In contrast, Cullen and Cousens (2024) report lower ^{87}Sr/^{86}Sr dispersion in tyrannosaurids compared to other taxa. Our study finds an ^{87}Sr/^{86}Sr SD of 0.00035 (or 0.00028 removing a low-radiogenic outlier) for tyrannosaurid enamel. Overall, our findings underscore the need for caution when interpreting radiogenic Sr isotopes in dinosaur teeth for migration

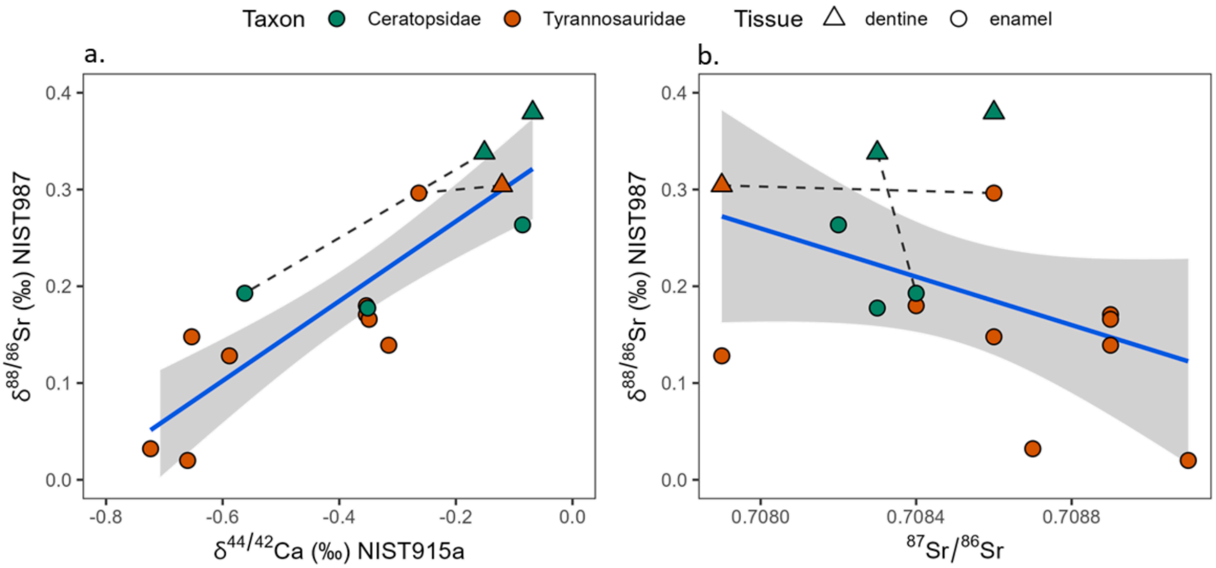

Fig. 10. Correlation plots between $\delta^{88/86}$Sr and $\delta^{44/42}$Ca (a.) and between $\delta^{88/86}$Sr and ^{87}Sr/^{86}Sr (b.) of dentine (triangles) and enamel (circles) from the analyzed tyrannosaurid (orange) and ceratopsid (green) teeth fragments. Samples from the same tooth are connected through a dashed line; blue lines are linear fits (R^2 $\delta^{44/42}$Ca vs $\delta^{88/86}$Sr = 0.76, p = 2.4e−05; R^2 $\delta^{88/86}$Sr vs ^{87}Sr/^{86}Sr = 0.19, p = 0.11) with their relative standard error as gray envelopes. Calcium isotope values are expressed as $\delta^{44/42}$Ca (‰), relative to NIST SRM 915a. Strontium isotope values are expressed as $\delta^{88/86}$Sr (‰), relative to NIST SRM 987.

or provenance, given the potential variability in diagenetic alteration across taxa.

6.4. *Geochemical significance and implications*

Integrating Ca and Sr (both stable and radiogenic) isotopes with trace elements sensitive to diagenesis, can significantly enhance our reconstruction of the taphonomic history of biological remains. In our study, the lack of typically negative $\delta^{88/86}$Sr values, indicative of biological fractionation processes, and the convergence towards geogenic values suggests diagenetic alteration. This observation raises concerns on the reliability of ^{87}Sr/^{86}Sr from fossil teeth for mobility studies. When the stable Sr isotope composition ($\delta^{88/86}$Sr) is heavily shifted towards positive geogenic values, it is likely that the corresponding radiogenic Sr isotope ratios are similarly compromised, hampering paleo-mobility reconstructions.

Mass bias modeling of $\delta^{44/42}$Ca and $\delta^{88/86}$Sr offers a useful perspective, revealing that diagenetically resistant Ca in tooth enamel appears less affected by *post mortem* alteration than Sr. Ca isotopic signals, supported by higher Ca content in enamel, retain a trophic shift comparable to that seen in modern unaltered materials, even if some alteration cannot be entirely ruled out.

Overall, our study demonstrates the potential of combining Ca isotopes with both stable and radiogenic Sr isotope studies to assess the preservation of biogenic signals in dinosaur teeth. Coupled with established trace element proxies, this integrated approach represents a promising diagenetic screening tool for fossil remains, potentially extending to other extinct taxa. Given the limited availability of well-preserved enamel and the destructive nature of these analyses, developing additional geochemical proxies to better understand taphonomic conditions is a key priority for future research. Our dataset not only contributes to reconstructing trophic relationships in extinct food chains, but also provides a foundation for further refinement and validation of this technique.

7. Conclusions

Our integrated geochemical approach yields several key insights. Tyrannosaurid enamel is less diagenetically altered than that of ceratopsids, likely due to its denser, less porous microstructure that limits the uptake of diagenetic elements (e.g., U, REE and others).

The Ca isotope composition in enamel shows evident diet-related differences, with tyrannosaurids being more ^{44}Ca-depleted, a pattern consistent with modern trophic level effects. In contrast, dentine shows higher levels of diagenetic trace elements and ^{44}Ca enrichment, which masks any trophic signal and makes it less useful for dietary reconstructions. Therefore enamel emerges as the more robust geochemical proxy archive for reconstructing dinosaur dietary and ecological niches.

Ca isotopes of tyrannosaurid teeth from the upper Oldman Formation suggest a potential prey preference for ceratopsids, although the variability of $\delta^{44/42}$Ca among taxa (e.g., ceratopsids and hadrosaurids) implies that environmental shifts and changes in food availability may have broadened tyrannosaurids diets, ultimately buffering isotopic signals. A positive correlation between $\delta^{44/42}$Ca and $\delta^{88/86}$Sr in both dentine and enamel possibly suggests similar biogeochemical fractionation along the food chain. However, Sr is more susceptible to diagenetic overprinting. While the original diet-related $\delta^{44/42}$Ca signal in enamel seems generally preserved, $\delta^{88/86}$Sr values trend towards more positive rock/soil-like compositions. Modeling based on modern fauna data, with a hypothetical $\delta^{88/86}$Sr diagenetic end-member of 0.40 ‰, suggests that diagenetic Sr may account for roughly 60–85 % of the total Sr in these teeth, urging caution in using Sr isotopes alone for mobility or dietary interpretations in deep time. Nevertheless, $\delta^{88/86}$Sr can serve as a sensitive indicator of diagenetic alteration, particularly reflecting the loss of biogenic, diet-derived negative $\delta^{88/86}$Sr signatures. Part of the original biogenic Sr isotope composition might still be retained within the best-preserved enamel samples.

To develop a more robust quantitative multi-proxy model of diagenetic alteration, future research should expand elemental and isotopic analyses across a broader range of taxa, creating comprehensive databases for ^{87}Sr/^{86}Sr, ^{88}Sr/^{86}Sr, ^{44}Ca/^{42}Ca and trace elements. In conclusion, our study underscores the need for a careful, multi-proxy approach, including a larger taxonomic dataset, to reliably disentangle biogenic signals from diagenetic overprinting in fossil remains.

CRediT authorship contribution statement

Mateusz M. Michailow: Writing – original draft, Methodology, Investigation, Formal analysis, Data curation. **Federico Lugli:** Writing –

original draft, Visualization, Validation, Supervision, Software, Project administration, Methodology, Investigation, Formal analysis, Data curation, Conceptualization. **Anna Cipriani:** Writing – original draft, Supervision, Resources, Investigation, Funding acquisition, Conceptualization. **Francesco Della Giustina:** Writing – review & editing, Formal analysis. **Annalisa Ferretti:** Writing – review & editing, Supervision, Resources, Funding acquisition, Formal analysis, Conceptualization. **Daniele Malferrari:** Writing – review & editing, Formal analysis, Data curation. **Denver Fowler:** Writing – review & editing, Resources. **Elizabeth Freedman Fowler:** Writing – review & editing, Resources. **Michael Weber:** Writing – review & editing, Resources, Methodology, Investigation, Formal analysis, Data curation. **Thomas Tütken:** Writing – review & editing, Visualization, Supervision, Resources, Project administration, Funding acquisition, Conceptualization.

Declaration of competing interest

The authors declare that they have no known competing financial interests or personal relationships that could have appeared to influence the work reported in this paper.

Acknowledgements

Tyrannosaurid and ceratopsid tooth fragments are courtesy of the Badlands Dinosaur Museum, Dickinson Museum Center (North Dakota, USA). Specimens collected under permit (#108829 (MT932.GAL) to DF, EAF) from US public lands administered by the US Bureau of Land Management. Special thanks to Greg Liggett and Josh Chase (BLM), the US Bureau of Reclamation, the Staples family and the Hilldale Hutterite colony, for assistance, camping permissions, and land access during fieldwork in Havre, Montana.

TT received funding from the European Research Council (ERC) under the European Union's Horizon 2020 research and innovation program grant agreement No 681450. MW was funded by DFG, Deutsche Forschungsgemeinschaft WE 7074/1-1 and INST 247/889 FUGG. FL received funding from the European Union's Horizon Europe research and innovation program under the Marie Skłodowska-Curie grant agreement No. 101104566 "AROUSE". This research was undertaken within the framework and with the financial support of the European Community – Next Generation EU, Italian Ministry of University and Research, Project P2022K9BE8, PRIN-PNRR 2022 "OCEANS" (AF) and Project 2022MAM9ZB, PRIN-2022 "BIOVERTICES" (AF).

We sincerely thank three anonymous reviewers and the associate editor – Prof. Elizabeth Griffith – for their thoughtful comments, which greatly improved the quality and clarity of this manuscript.

Appendix A. Supplementary material

The supplementary material includes isotope and elemental data plots, showing $\delta^{44/42}$Ca vs $\delta^{43/42}$Ca, Y/Ho vs Sm_N/Yb_N and Ce/Ce*vs Pr/Pr* plots, and NASC normalized La/Sm and La/Yb ratios for tyrannosaurid and ceratopsid teeth, compared to previous studies. A set of SEM pictures from literature illustrates differences in enamel microstructure of the analyzed dinosaur taxa. It also presents Ca isotope composition of dentine and enamel pairs, and U-Sr and ΣREE-Sr biplots distinguishing enamel and dentine samples, along with a table listing the trace elemental content of analyzed teeth. Supplementary material to this article can be found online at https://doi.org/10.1016/j.gca.2025.05.006.

Data availability

All data are available at Zenodo: https://doi.org/10.5281/zenodo.12699476.

References

Argentino, C., Lugli, F., Cipriani, A., Panieri, G., 2021. Testing miniaturized extraction chromatography protocols for combined ^{87}Sr/^{86}Sr and $\delta^{88/86}$Sr analyses of pore water by MC-ICP-MS. Limnol. Oceanogr. Methods 19, 431–440.

Ayliffe, L.K., Chivas, A.R., Leakey, M.G., 1994. The retention of primary oxygen isotope compositions of fossil elephant skeletal phosphate. Geochim. Cosmochim. Acta 58, 5291–5298.

Ballell, A., Benton, M.J., Rayfield, E.J., 2022. Dental form and function in the early feeding diversification of dinosaurs. Sci. Adv. 8, eabq5201.

Balter, V., 2004. Allometric constraints on Sr/Ca and Ba/Ca partitioning in terrestrial mammalian trophic chains. Oecologia 139, 83–88.

Balter, V., Martin, J.E., Tacail, T., Suan, G., Renaud, S., Girard, C., 2019. Calcium stable isotopes place Devonian conodonts as first level consumers. Geochem. Perspect. Lett. 36–39.

Bentley, R.A., 2006. Strontium isotopes from the earth to the archaeological skeleton: a review. J. Archaeol. Method Theory 13, 135–187.

Bocherens, H., Brinkman, D.B., Dauphin, Y., Mariotti, A., 1994. Microstructural and geochemical investigations on Late Cretaceous archosaur teeth from Alberta, Canada. Can. J. Earth Sci. 31, 783–792.

Boer, W., Nordstad, S., Weber, M., Mertz-Kraus, R., Hönisch, B., Bijma, J., Raitzsch, M., Wilhelms-Dick, D., Foster, G.L., Goring-Harford, H., Nürnberg, D., Hauff, F., Kuhnert, H., Lugli, F., Spero, H., Rosner, M., van Gaever, P., de Nooijer, L.J., Reichart, G., 2022. New calcium carbonate nano-particulate pressed powder pellet (NFHS-2-NP) for LA-ICP-OES, LA-(MC)-ICP-MS and µXRF. Geostand. Geoanal. Res. 46, 411–432.

Bourgon, N., Jaouen, K., Bacon, A.-M., Dufour, E., McCormack, J., Tran, N.-H., Trost, M., Fiorillo, D., Dunn, T.E., Zanolli, C., Zachwieja, A., Duringer, P., Ponche, J.-L., Boesch, Q., Antoine, P.-O., Westaway, K.E., Joannes-Boyau, R., Suzzoni, E., Frangeul, S., Crozier, F., Aubaile, F., Patole-Edoumba, E., Luangkhoth, T., Souksavatdy, V., Boualaphane, S., Sayavonkhamdy, T., Sichanthongtip, P., Sihanam, D., Demeter, F., Shackelford, L.L., Hublin, J.-J., Tütken, T., 2021. Trophic ecology of a Late Pleistocene early modern human from tropical Southeast Asia inferred from zinc isotopes. J. Hum. Evol. 161, 103075.

Burton, J.H., Price, T.D., Middleton, W.D., 1999. Correlation of bone Ba/Ca and Sr/Ca due to biological purification of calcium. J. Archaeol. Sci. 26, 609–616.

Chao, H.C., You, C.F., Liu, H.C., Chung, C.H., 2015. Evidence for stable Sr isotope fractionation by silicate weathering in a small sedimentary watershed in southwestern Taiwan. Geochim. Cosmochim. Acta 165, 324–341.

Chin, K., Eberth, D.A., Schweitzer, M.H., Rando, T.A., Sloboda, W.J., Horner, J.R., 2003. Remarkable preservation of undigested muscle tissue within a Late Cretaceous Tyrannosaurid Coprolite from Alberta, Canada. PALAIOS 18, 286–294.

Chin, K., Tokaryk, T.T., Erickson, G.M., Calk, L.C., 1998. A king-sized theropod coprolite. Nature 393, 680–682.

Chu, N.-C., Henderson, G.M., Belshaw, N.S., Hedges, R.E.M., 2006. Establishing the potential of Ca isotopes as proxy for consumption of dairy products. Appl. Geochem. 21, 1656–1667.

Clementz, M.T., Hoppe, K.A., Koch, P.L., 2003. A Paleoecological paradox: the habitat and dietary preferences of the extinct tethythere desmostylus, inferred from stable isotope analysis. Paleobiology 29, 506–519.

Clementz, M.T., 2012. New insight from old bones: stable isotope analysis of fossil mammals. J. Mammal. 93, 368–380.

Cobert, F., Schmitt, A.-D., Bourgeade, P., Labolle, F., Badot, P.-M., Chabaux, F., Stille, P., 2011. Experimental identification of Ca isotopic fractionations in higher plants. Geochim. Cosmochim. Acta 75, 5467–5482.

Cullen, T.M., Cousens, B.L., 2024. New biogeochemical insights into Mesozoic terrestrial paleoecology and evidence for omnivory in troodontid dinosaurs. GSA Bull. 136, 2689–2701.

Cullen, T.M., Zhang, S., Spencer, J., Cousens, B., 2022. Sr-O-C isotope signatures reveal herbivore niche-partitioning in a Cretaceous ecosystem. Palaeontology 65, e12591.

Currie, P.J., Rigby, J.K., Sloan, R.E., 1990. Theropod teeth from the Judith River Formation of southern Alberta, Canada. In: Carpenter, K., Currie, P.J. (Eds.), Dinosaur Systematics: Approaches and Perspectives. Cambridge University Press, Cambridge, pp. 107–126.

De Souza, G.F., Reynolds, B.C., Kiczka, M., Bourdon, B., 2010. Evidence for mass-dependent isotopic fractionation of strontium in a glaciated granitic watershed. Geochim. Cosmochim. Acta 74, 2596–2614.

Dodat, P.-J., Martin, J.E., Olive, S., Hassler, A., Albalat, E., Boisserie, J.-R., Merceron, G., Souron, A., Maureille, B., Balter, V., 2023. Limits of calcium isotopes diagenesis in fossil bone and enamel. Geochim. Cosmochim. Acta 351, 45–50.

Dodson, P., Forster, C.A., Sampson, S.D., 2004. Ceratopsidae. In: Weishampel, D. (Ed.), The Dinosauria. University of California Press. pp. 494–513.

Eberth, D.A., 2005. The geology. In: Currie, P.J., Koppelhus, E.B. (Eds.), Dinosaur Provincial Park: A Spectacular Ancient Ecosystem Revealed. Indiana University Press, Bloomington, Indiana, pp. 54–82.

Eberth, D.A., Hamblin, A.P., 1993. Tectonic, stratigraphic, and sedimentologic significance of a regional discontinuity in the upper Judith River Group (Belly River wedge) of southern Alberta, Saskatchewan, and northern Montana. Can. J. Earth Sci. 30, 174–200.

Eberth, D.A., 2024. Stratigraphic architecture of the Belly River Group (Campanian, Cretaceous) in the plains of southern Alberta: Revisions and updates to an existing model and implications for correlating dinosaur-rich strata ed. J. Kriwet. PLoS ONE 19, e0292318.

Elderfield, H., Pagett, R., 1986. Rare earth elements in ichthyoliths: Variations with redox conditions and depositional environment. Sci. Total Environ. 49, 175–197.

Elderfield, H., Upstill-Goddard, R., Sholkovitz, E.R., 1990. The rare earth elements in rivers, estuaries, and coastal seas and their significance to the composition of ocean waters. Geochim. Cosmochim. Acta 54, 971–991.

Elias, R.W., Hirao, Y., Patterson, C.C., 1982. The circumvention of the natural biopurification of calcium along nutrient pathways by atmospheric inputs of industrial lead. Geochim. Cosmochim. Acta 46, 2561–2580.

Erickson, G.M., Kirk, S.D.V., Su, J., Levenston, M.E., Caler, W.E., Carter, D.R., 1996. Bite-force estimation for Tyrannosaurus rex from tooth-marked bones. Nature 382, 706–708.

Erickson, G.M., Krick, B.A., Hamilton, M., Bourne, G.R., Norell, M.A., Lilleodden, E., Sawyer, W.G., 2012. Complex dental structure and wear biomechanics in hadrosaurid dinosaurs. Science 338, 98–101.

Ericson, J.E., 1985. Strontium isotope characterization in the study of prehistoric human ecology. J. Hum. Evol. 14, 503–514.

Fiorillo, A., Currie, P., 1994. Theropod teeth from the Judith River Formation (Upper Cretaceous) of South-Central Montana. J. Vertebr. Paleontol. 14, 74–80.

Fischer, J., Voigt, S., Franz, M., Schneider, J.W., Joachimski, M.M., Tichomirowa, M., Götze, J., Furrer, H., 2012. Palaeoenvironments of the late Triassic Rhaetian Sea: implications from oxygen and strontium isotopes of hybodont shark teeth. Palaeogeogr. Palaeoclimatol. Palaeoecol. 353–355, 60–72.

Fowler, D.W., 2017. Revised geochronology, correlation, and dinosaur stratigraphic ranges of the Santonian-Maastrichtian (Late Cretaceous) formations of the Western Interior of North America ed. W. O. Wong. PLoS ONE 12, e0188426.

Fricke, H.C., Rogers, R.R., Backlund, R., Dwyer, C.N., Echt, S., 2008. Preservation of primary stable isotope signals in dinosaur remains, and environmental gradients of the Late Cretaceous of Montana and Alberta. Palaeogeogr. Palaeoclimatol. Palaeoecol. 266, 13–27.

Gannes, L.Z., del Rio, C.M., Koch, P., 1998. Natural abundance variations in stable isotopes and their potential uses in animal physiological ecology. Comp. Biochem. Physiol. A Mol. Integr. Physiol. 119, 725–737.

Gatti, L., Lugli, F., Sciutto, G., Zangheri, M., Prati, S., Mirasoli, M., Silvestrini, S., Benazzi, S., Tütken, T., Douka, K., Collina, C., Boschin, F., Romandini, M., Iacumin, P., Guardigli, M., Roda, A., Mazzeo, R., 2022. Combining elemental and immunochemical analyses to characterize diagenetic alteration patterns in ancient skeletal remains. Sci. Rep. 12, 5112.

Giblin, A.M., Dickson, B.L., 1992. Source, distribution and economic significance of trace elements in groundwaters from Lake Tyrrell, Victoria, Australia. Chem. Geol. 96, 133–149.

Gignac, P.M., Erickson, G.M., 2017. The biomechanics behind extreme osteophagy in Tyrannosaurus rex. Sci. Rep. 7, 2012.

Giovanardi, T., Mazzucchelli, M., Lugli, F., Girardi, V.A., Correia, C.T., Tassinari, C.C., Cipriani, A., 2018. Isotopic constraints on contamination processes in the Tonian Goiás Stratiform Complex. Lithos 310, 136–152.

Grandjean, P., 1989. Les terres rares et la composition isotopique du néodyme dans les phosphates biogènes: traceurs des processus paléo-océanographiques et sédimentaires (Doctoral dissertation, Vandoeuvre-les-Nancy, INPL).

Grandjean, P., Albarède, F., 1989. Ion probe measurement of rare earth elements in biogenic phosphates. Geochimica et Cosmochimica Acta 53, 3179–3183.

Grandjean, P., Cappetta, H., Albarède, F., 1988. The REE and ε_{Nd} of 40-70 Ma old fish debris from the west-African platform. Geophys. Res. Lett. 15, 389–392.

Gueriau, P., Mocuta, C., Dutheil, D.B., Cohen, S.X., Thiaudière, D., The OT1 Consortium, Charbonnier, S., Clément, G., Bertrand, L., 2014. Trace elemental imaging of rare earth elements discriminates tissues at microscale in flat fossils ed. E. A. Rozhkova. PLoS ONE 9, e86946.

Guiserix, D., Dodat, P.J., Jaouen, K., Albalat, E., Cardoso, J.M., Maureille, B., Balter, V., 2024. Stable isotope composition and concentration systematics of Ca and trace elements (Zn, Sr) in single aliquots of fossil bone and enamel. Geochim. Cosmochim. Acta 367, 123–132.

Hajj, F., Poszwa, A., Bouchez, J., Guérold, F., 2017. Radiogenic and "stable" strontium isotopes in provenance studies: a review and first results on archaeological wood from shipwrecks. J. Archaeol. Sci. 86, 24–49.

Hamblin, A.P., Abrahamson, B.W., 1996. Stratigraphic architecture of "Basal Belly River" cycles, Foremost Formation, Belly River Group, subsurface of southern Alberta and southwestern Saskatchewan. Bull. Can. Pet. Geol. 44, 654–673.

Hassler, A., Martin, J.E., Amiot, R., Tacail, T., Godet, F.A., Allain, R., Balter, V., 2018. Calcium isotopes offer clues on resource partitioning among Cretaceous predatory dinosaurs. Proc. R. Soc. B Biol. Sci. 285, 20180197.

Hassler, A., Martin, J.E., Merceron, G., Garel, M., Balter, V., 2021. Calcium isotopic variability of cervid bioapatite and implications for mammalian physiology and diet. Palaeogeogr. Palaeoclimatol. Palaeoecol. 573, 110418.

Hedges, R.E.M., Stevens, R.E., Pearson, J., 2006. Carbon and nitrogen stable isotope compositions of animal and human bone. In: Building Memories: The Neolithic Cotswold Long Barrow at Ascott-under-Wychwood, Oxfordshire. Don Benson, Alasdair Whittle. pp. 255–262.

Herwartz, D., Tütken, T., Jochum, K.P., Sander, P.M., 2013. Rare earth element systematics of fossil bone revealed by LA-ICPMS analysis. Geochim. Cosmochim. Acta 103, 161–183.

Herwartz, D., Tütken, T., Münker, C., Jochum, K.P., Stoll, B., Sander, P.M., 2011. Timescales and mechanisms of REE and Hf uptake in fossil bones. Geochim. Cosmochim. Acta 75, 82–105.

Heuser, A., Tütken, T., Gussone, N., Galer, S.J.G., 2011. Calcium isotopes in fossil bones and teeth — diagenetic versus biogenic origin. Geochim. Cosmochim. Acta 75, 3419–3433.

Hone, D.W.E., Tanke, D.H., Brown, C.M., 2018. Bite marks on the frill of a juvenile Centrosaurus from the Late Cretaceous Dinosaur Provincial Park Formation, Alberta, Canada. Peerj 6, e5748.

Hoppe, K.A., Koch, P.L., Carlson, R.W., Webb, S.D., 1999. Tracking mammoths and mastodons: reconstruction of migratory behavior using strontium isotope ratios. Geology 27, 439–442.

Hubert, J.F., Panish, P.T., Chure, D.J., Prostak, K., 1996. Chemistry, microstructure, petrology, and diagenetic model of Jurassic Dinosaur Bones, Dinosaur National Monument, Utah. J. Sediment. Res. 66, 531–547.

Hwang, S.H., 2005. Phylogenetic patterns of enamel microstructure in dinosaur teeth. J. Morphol. 266, 208–240.

Hwang, S.H., 2010. The utility of tooth enamel microstructure in identifying isolated dinosaur teeth. Lethaia 43, 307–322.

Hwang, S.H., 2011. The evolution of dinosaur tooth enamel microstructure. Biol. Rev. 86, 183–216.

Jacobsen, A.R., 1998. Feeding behaviour of carnivorous dinosaurs as determined by tooth marks on dinosaur bones. Hist. Biol. 13, 17–26.

Jaouen, K., Pons, M.-L., 2017. Potential of non-traditional isotope studies for bioarchaeology. J. Anthropol. Archaeol. Sci. 9, 1389–1404.

Jerzykiewicz, T., Norris, D.K., 1994. Stratigraphy, structure and syntectonic sedimentation of the Campanian "Belly River" clastic wedge in the southern Canadian Cordillera. Cretac. Res. 15, 367–399.

Johannesson, K.H., Lyons, W.B., 1995. Rare-earth element geochemistry of Colour Lake, an acidic freshwater lake on Axel Heiberg Island, Northwest Territories, Canada. Chem. Geol. 119, 209–223.

Kauffman, E.G., 1984. Paleobiogeography and evolutionary response dynamic in the Cretaceous Western Interior Seaway of North America. Geol. Assoc. Can. Spec. Pap. 27, 273–306.

Knudson, K.J., Williams, H.M., Buikstra, J.E., Tomczak, P.D., Gordon, G.W., Anbar, A.D., 2010. Introducing $\delta^{88/86}$Sr analysis in archaeology: a demonstration of the utility of strontium isotope fractionation in paleodietary studies. J. Archaeol. Sci. 37, 2352–2364.

Koch, P.L., 2007. Isotopic study of the biology of modern and fossil vertebrates. In: Michener, R., Lajtha, K. (Eds.), Stable Isotopes in Ecology and Environmental Science. John Wiley & Sons, pp. 99–154.

Kocsis, L., Gheerbrant, E., Mouflih, M., Cappetta, H., Ulianov, A., Chiaradia, M., Bardet, N., 2016. Gradual changes in upwelled seawater conditions (redox, pH) from the late Cretaceous through early Paleogene at the northwest coast of Africa: Negative Ce anomaly trend recorded in fossil bio-apatite. Chem. Geol. 421, 44–54.

Kocsis, L., Ősi, A., Vennemann, T., Trueman, C.N., Palmer, M.R., 2009. Geochemical study of vertebrate fossils from the Upper Cretaceous (Santonian) Csehbánya Formation (Hungary): evidence for a freshwater habitat of mosasaurs and pycnodont fish. Palaeogeogr. Palaeoclimatol. Palaeoecol. 280, 532–542.

Kohn, M.J., Cerling, T.E., 2002. Stable isotope compositions of biological apatite. Rev. Mineral. Geochem. 48, 455–488.

Kohn, M.J., Schoeninger, M.J., Barker, W.W., 1999. Altered states: effects of diagenesis on fossil tooth chemistry. Geochim. Cosmochim. Acta 63, 2737–2747.

Kohn, M.J., Morris, J., Olin, P., 2013. Trace element concentrations in teeth–a modern Idaho baseline with implications for archeometry, forensics, and palaeontology. J. Archaeol. Sci. 40, 1689–1699.

Kolodny, Y., Luz, B., Sander, M., Clemens, W.A., 1996. Dinosaur bones: fossils or pseudomorphs? The pitfalls of physiology reconstruction from apatitic fossils. Palaeogeogr. Palaeoclimatol. Palaeoecol. 126, 161–171.

Kowal-Linka, M., Jochum, K.P., Surmik, D., 2014. LA-ICP-MS analysis of rare earth elements in marine reptile bones from the Middle Triassic bonebed (Upper Silesia, S Poland): Impact of long-lasting diagenesis, and factors controlling the uptake. Chem. Geol. 363, 213–228.

Kral, A.G., Lagos, M., Guagliardo, P., Tütken, T., Geisler, T., 2022. Rapid alteration of cortical bone in fresh- and seawater solutions visualized and quantified from the millimeter down to the atomic scale. Chem. Geol. 609, 121060.

Kral, A.G., Geisler, T., Wiedenbeck, M., Guagliardo, P., Tütken, T., 2024. Phosphate uptake is an essential process for rapid bone mineralization during early diagenesis–evidence from bone alteration experiments. Geochim. Cosmochim. Acta 375, 173–185.

LeBlanc, A.R.H., Apesteguía, S., Larsson, H.C.E., Caldwell, M.W., 2020. Unique Tooth Morphology and Prismatic Enamel in Late Cretaceous Sphenodontians from Argentina. Curr. Biol. 30, 1755–1761.

Lee-Thorp, J., Sponheimer, M., 2006. Contributions of biogeochemistry to understanding hominin dietary ecology. Am. J. Phys. Anthropol. 131, 131–148.

Leichliter, J.N., Lüdecke, T., Foreman, A.D., Duprey, N.N., Winkler, D.E., Kast, E.R., et al., 2021. Nitrogen isotopes in tooth enamel record diet and trophic level enrichment: results from a controlled feeding experiment. Chem. Geol. 563, 120047.

Leichliter, J.N., Lüdecke, T., Foreman, A.D., Bourgon, N., Duprey, N.N., Vonhof, H., et al., 2023. Tooth enamel nitrogen isotope composition records trophic position: a tool for reconstructing food webs. Commun. Biol. 6, 373.

Longerich, H.P., Jackson, S.E., Günther, D., 1996. Inter-laboratory note. Laser ablation inductively coupled plasma mass spectrometric transient signal data acquisition and analyte concentration calculation. J. Anal. At. Spectrom 11, 899–904.

Longrich, N.R., Horner, J.R., Erickson, G.M., Currie, P.J., 2010. Cannibalism in Tyrannosaurus rex ed. A. A. Farke. PLoS ONE 5, e13419.

Lugli, F., Cipriani, A., Capecchi, G., Ricci, S., Boschin, F., Boscato, P., Iacumin, P., Badino, F., Mannino, M.A., Talamo, S., Richards, M.P., Benazzi, S., Ronchitelli, A., 2019. Strontium and stable isotope evidence of human mobility strategies across the Last Glacial Maximum in southern Italy. Nat. Ecol. Evol. 3, 905–911.

Lugli, F., Cipriani, A., Tavaglione, V., Traversari, M., Benazzi, S., 2018. Transhumance pastoralism of Roccapelago (Modena, Italy) Early-Modern individuals: inferences from Sr isotopes of hair strands. Am. J. Phys. Anthropol. 167, 470–483.

Lyson, T.R., Longrich, N.R., 2011. Spatial niche partitioning in dinosaurs from the latest cretaceous (Maastrichtian) of North America. Proc. R. Soc. B Biol. Sci. 278, 1158–1164.

Maiorino, L., Farke, A.A., Kotsakis, T., Teresi, L., Piras, P., 2015. Variation in the shape and mechanical performance of the lower jaws in ceratopsid dinosaurs (Ornithischia, Ceratopsia). J. Anat. 227, 631–646.

Makovicky, P.J., 2012. Marginocephalia. In: The Complete Dinosaur. In: Brett-Surman, M.K., Holtz, T.R. Jr., Farlow, J.O. (Eds), Indiana University Press, Bloomington, IN, pp. 527–549.

Mallon, J.C., Anderson, J.S., 2014. The functional and palaeoecological implications of tooth morphology and wear for the Megaherbivorous Dinosaurs from the Dinosaur Park Formation (Upper Campanian) of Alberta, Canada. PLoS One 9, e98605.

Mallon, J.C., Anderson, J.S., 2015. Jaw mechanics and evolutionary paleoecology of megaherbivorous dinosaurs from the Dinosaur Park Formation (upper Campanian) of Alberta, Canada. J. Vertebr. Paleontol. 35, 1–17.

Martin, J.E., Deesri, U., Liard, R., Wattanapituksakul, A., Suteethorn, S., Lauprasert, K., Tong, H., Buffetaut, E., Suteethorn, V., Suan, G., Telouk, P., Balter, V., 2016. Strontium isotopes and the long-term residency of thalattosuchians in the freshwater environment. Paleobiology 42, 143–156.

Martin, J.E., Hassler, A., Montagnac, G., Therrien, F., Balter, V., 2022. The stability of dinosaur communities before the Cretaceous–Paleogene (K–Pg) boundary: A perspective from southern Alberta using calcium isotopes as a dietary proxy. Geol. Soc. Am. Bull. 134, 2548–2560.

Martin, J.E., Tacail, T., Balter, V., 2017. Non-traditional isotope perspectives in vertebrate palaeobiology ed. A. Smith. Palaeontology 60, 485–502.

Martin, J.E., Tacail, T., Adnet, S., Girard, C., Balter, V., 2015. Calcium isotopes reveal the trophic position of extant and fossil elasmobranchs. Chem. Geol. 415, 118–125.

Martin, J.E., Tacail, T., Cerling, T.E., Balter, V., 2018. Calcium isotopes in enamel of modern and Plio-Pleistocene East African mammals. Earth Planet. Sci. Lett. 503, 227–235.

McArthur, J.M., Howarth, R.J., Bailey, T.R., 2001. Strontium isotope stratigraphy: LOWESS version 3: best fit to the marine Sr-isotope curve for 0–509 Ma and accompanying look-up table for deriving numerical age. J. Geol. 109, 155–170.

McCormack, J., Griffiths, M.L., Kim, S.L., Shimada, K., Karnes, M., Maisch, H., Pederzani, S., Bourgon, N., Jaouen, K., Becker, M.A., Jöns, N., Sisma-Ventura, G., Straube, N., Pollerspöck, J., Hublin, J.-J., Eagle, R.A., Tütken, T., 2022. Trophic position of Otodus megalodon and great white sharks through time revealed by zinc isotopes. Nat. Commun. 13, 2980.

Medici, L., Savioli, M., Ferretti, A., Malferrari, D., 2021. Zooming in REE and other trace elements on conodonts: does taxonomy guide diagenesis? J. Earth Sci. 32, 501–511.

Millard, A.R., Hedges, R.E.M., 1996. A diffusion-adsorption model of uranium uptake by archaeological bone. Geochim. Cosmochim. Acta 60, 2139–2152.

Minagawa, M., Wada, E., 1984. Stepwise enrichment of 15N along food chains: further evidence and the relation between δ15N and animal age. Geochim. Cosmochim. Acta 48, 1135–1140.

Montanari, S., Higgins, P., Norell, M.A., 2013. Dinosaur eggshell and tooth enamel geochemistry as an indicator of Mongolian Late Cretaceous paleoenvironments. Palaeogeogr. Palaeoclimatol. Palaeoecol. 370, 158–166.

Moynier, F., Fujii, T., 2017. Calcium isotope fractionation between aqueous compounds relevant to low-temperature geochemistry, biology and medicine. Sci. Rep. 7, 44255.

Nardelli, M.P., Malferrari, D., Ferretti, A., Bartolini, A., Sabbatini, A., Negri, A., 2016. Zinc incorporation in the miliolid foraminifer Pseudotriloculina rotunda under laboratory conditions. Mar. Micropaleontol. 126, 42–49.

Nava, A., Lugli, F., Romandini, M., Badino, F., Evans, D., Helbling, A.H., Oxilia, G., Arrighi, S., Bortolini, E., Delpiano, D., Duches, R., Figus, C., Livraghi, A., Marciani, G., Silvestrini, S., Cipriani, A., Giovanardi, T., Pini, R., Tuniz, C., Bernardini, F., Dori, I., Coppa, A., Cristiani, E., Dean, C., Bondioli, L., Peresani, M., Müller, W., Benazzi, S., 2020. Early life of Neanderthals. Proc. Natl. Acad. Sci. 117, 28719–28726.

Newsome, S., Clementz, M., Koch, P., 2010. Using stable isotope biogeochemistry to study marine mammal ecology. Mar. Mamm. Sci. 26, 509–572.

Ostrom, J.H., 1966. Functional morphology and evolution of the ceratopsian dinosaurs. Evolution 20, 290–308.

Pasteris, J.D., Wopenka, B., Valsami-Jones, E., 2008. Bone and tooth mineralization: why apatite? Elements 4, 97–104.

Pfretzschner, H.-U., 2004. Fossilization of Haversian bone in aquatic environments. C.R. Palevol 3, 605–616.

Ramezani, J., Beveridge, T.L., Rogers, R.R., Eberth, D.A., Roberts, E.M., 2022. Calibrating the zenith of dinosaur diversity in the Campanian of the Western Interior Basin by CA-ID-TIMS U–Pb geochronology. Sci. Rep. 12, 16026.

Rey, L., Tacail, T., Santos, F., Rottier, S., Goude, G., Balter, V., 2022. Disentangling diagenetic and biogenic trace elements and Sr radiogenic isotopes in fossil dental enamel using laser ablation analysis. Chem. Geol. 587, 120608.

Reynard, B., Balter, V., 2014. Trace elements and their isotopes in bones and teeth: Diet, environments, diagenesis, and dating of archeological and paleontological samples. Palaeogeogr. Palaeoclimatol. Palaeoecol. 416, 4–16.

Reynard, B., Lécuyer, C., Grandjean, P., 1999. Crystal-chemical controls on rare-earth element concentrations in fossil biogenic apatites and implications for paleoenvironmental reconstructions. Chem. Geol. 155, 233–241.

Reynard, L.M., Henderson, G.M., Hedges, R.E.M., 2010. Calcium isotope ratios in animal and human bone. Geochim. Cosmochim. Acta 74, 3735–3750.

Reynard, L.M., Henderson, G.M., Hedges, R.E.M., 2011. Calcium isotopes in archaeological bones and their relationship to dairy consumption. J. Archaeol. Sci. 38, 657–664.

Rogers, R.R., 1998. Sequence analysis of the Upper Cretaceous Two Medicine and Judith River formations, Montana; nonmarine response to the Claggett and Bearpaw marine cycles. J. Sediment. Res. 68, 615–631.

Rogers, R.R., Eberth, D.A., Ramezani, J., 2023. The "Judith River−Belly River problem" revisited (Montana-Alberta-Saskatchewan): New perspectives on the correlation of Campanian dinosaur-bearing strata based on a revised stratigraphic model updated with CA-ID-TIMS U-Pb geochronology. Geol. Soc. Am. Bull. 136, 1221–1237.

Rogers, R.R., Kidwell, S.M., Deino, A.L., Mitchell, J.P., Nelson, K., Thole, J.T., 2016. Age, Correlation, and Lithostratigraphic Revision of the Upper Cretaceous (Campanian) Judith River Formation in Its Type Area (North-Central Montana), with a Comparison of Low- and High-Accommodation Alluvial Records. J. Geol. 124, 99–135.

Romaniello, S.J., Field, M.P., Smith, H.B., Gordon, G.W., Kim, M.H., Anbar, A.D., 2015. Fully automated chromatographic purification of Sr and Ca for isotopic analysis. J. Anal. At. Spectrom 30, 1906–1912.

Rowe, A.G., Bataille, C.P., Baleka, S., Combs, E.A., Crass, B.A., Fisher, D.C., Ghosh, S., Holmes, C.E., Krasinski, K.E., Lanoë, F., Murchie, T.J., Poinar, H., Potter, B., Rasic, J. T., Reuther, J., Smith, G.M., Spaleta, K.J., Wygal, B.T., Wooller, M.J., 2024. A female woolly mammoth's lifetime movements end in an ancient Alaskan hunter-gatherer camp. Sci. Adv. 10, eadk0818.

Sahni, A., 1972. The Vertebrate Fauna of the Judith River Formation, Montana. Bull. Am. Mus. Nat. Hist. 147, 325–412.

Sampson, S.D., Loewen, M.A., Farke, A.A., Roberts, E.M., Forster, C.A., Smith, J.A., Titus, A.L., 2010. New Horned Dinosaurs from Utah Provide Evidence for Intracontinental Dinosaur Endemism. PLoS One 5, e12292.

Sander, P., 1999. The microstructure of reptilian tooth enamel: Terminology, function, and phylogeny. Münchner Geowissenschaftliche Abhandlungen 38, 1–102.

Schmitt, A.-D., Vigier, N., Lemarchand, D., Millot, R., Stille, P., Chabaux, F., 2012. Processes controlling the stable isotope compositions of Li, B, Mg and Ca in plants, soils and waters: a review. C. R. Geosci. 344, 704–722.

Sharp, Z.D., Atudorei, V., Furrer, H., 2000. The effect of diagenesis on oxygen isotope ratios of biogenic phosphates. Am. J. Sci. 300, 222–237.

Skulan, J., DePaolo, D.J., 1999. Calcium isotope fractionation between soft and mineralized tissues as a monitor of calcium use in vertebrates. Proc. Natl. Acad. Sci. 96, 13709–13713.

Skulan, J.L., DePaolo, D.J., Owens, T.L., 1997. Biological control of calcium isotopic abundances in the global calcium cycle. Geochim. Cosmochim. Acta 61, 2505–2510.

Smedley, P.L., Kinniburgh, D.G., 2023. Uranium in natural waters and the environment: Distribution, speciation and impact. Appl. Geochem. 148, 105534.

Tacail, T., Albalat, E., Télouk, P., Balter, V., 2014. A simplified protocol for measurement of Ca isotopes in biological samples. J. Anal. At. Spectrom 29, 529.

Tacail, T., Le Houedec, S., Skulan, J.L., 2020. New frontiers in calcium stable isotope geochemistry: Perspectives in present and past vertebrate biology. Chem. Geol. 537, 119471.

Terrill, D.F., Henderson, C.M., Anderson, J.S., 2020. New application of strontium isotopes reveals evidence of limited migratory behaviour in Late Cretaceous hadrosaurs. Biol. Lett. 16, 20190930.

Therrien, F., Zelenitsky, D.K., Tanaka, K., Voris, J.T., Erickson, G.M., Currie, et al., 2023. Exceptionally preserved stomach contents of a young tyrannosaurid reveal an ontogenetic dietary shift in an iconic extinct predator. Sci. Adv. 9, eadi0505.

Thorp, J., Vandermerwe, N., 1987. Carbon Isotope Analysis of Fossil Bone Apatite. S. Afr. J. Sci. 83, 712–715.

Trueman, C.N., Tuross, N., 2002. Trace Elements in Recent and Fossil Bone Apatite. Rev. Mineral. Geochem. 48, 489–521.

Trueman, C., Chenery, C., Eberth, D.A., Spiro, B., 2003. Diagenetic effects on the oxygen isotope composition of bones of dinosaurs and other vertebrates recovered from terrestrial and marine sediments. J. Geol. Soc. London 160, 895–901.

Trueman, C.N., Behrensmeyer, A.K., Potts, R., Tuross, N., 2006. High-resolution records of location and stratigraphic provenance from the rare earth element composition of fossil bones. Geochim. Cosmochim. Acta 70, 4343–4355.

Trueman, C.N., Palmer, M.R., Field, J., Privat, K., Ludgate, N., Chavagnac, V., Eberth, D. A., Cifelli, R., Rogers, R.R., 2008a. Comparing rates of recrystallisation and the potential for preservation of biomolecules from the distribution of trace elements in fossil bones. C.R. Palevol 7, 145–158.

Trueman, C.N., Privat, K., Field, J., 2008b. Why do crystallinity values fail to predict the extent of diagenetic alteration of bone mineral? Palaeogeogr. Palaeoclimatol. Palaeoecol. 266, 160–167.

Tütken, T., Held, P., Herrmann, S., Galer, S.J.G., 2015. Combined $\delta^{88/86}$Sr and ^{87}Sr/^{86}Sr in bones and teeth: a toolbox for diet and habitat reconstruction. Goldschmidt Conference, Prag, Gold2015:abs: 3579.

Tütken, T., Vennemann, T.W., 2011. Fossil bones and teeth: preservation or alteration of biogenic compositions? Palaeogeogr. Palaeoclimatol. Palaeoecol. 310, 1–8.

Wang, Y., Cerling, T.E., 1994. A model of fossil tooth and bone diagenesis: implications for paleodiet reconstruction from stable isotopes. Palaeogeogr. Palaeoclimatol. Palaeoecol. 107, 281–289.

Weber, K., Weber, M., Menneken, M., Kral, A.G., Mertz-Kraus, R., Geisler, T., Vogl, J., Tütken, T., 2021. Diagenetic stability of non-traditional stable isotope systems (Ca, Sr, Mg, Zn) in teeth – An in-vitro alteration experiment of biogenic apatite in isotopically enriched tracer solution. Chem. Geol. 572, 120196.

Weber, M., Weber, K., Winkler, D., Tütken, T., 2025. Calcium and strontium isotopes in extant diapsid reptiles reflect dietary tendencies – a reference frame for diet reconstructions in the fossil record. Proc. R. Soc. B.

Weiner, S., Price, P.A., 1986. Disaggregation of bone into crystals. Calcif. Tissue Int. 39, 365–375.

Wooller, M.J., Bataille, C., Druckenmiller, P., Erickson, G.M., Groves, P., Haubenstock, N., Howe, T., Irrgeher, J., Mann, D., Moon, K., Potter, B.A., Prohaska, T., Rasic, J., Reuther, J., Shapiro, B., Spaleta, K.J., Willis, A.D., 2021. Lifetime mobility of an Arctic woolly mammoth. Science 373, 806–808.

Xu, X., Wang, K., Zhao, X., Li, D., 2010. First ceratopsid dinosaur from China and its biogeographical implications. Chin. Sci. Bull. 55, 1631–1635.